frontiers | Frontiers in Earth Science

TYPE Original Research
PUBLISHED 08 February 2023
DOI 10.3389/feart.2023.1091424

OPEN ACCESS

EDITED BY
Piotr Krzywiec,
Institute of Geological Sciences, Polish Academy of Sciences, Poland

REVIEWED BY
Dongya Zhu,
SINOPEC Petroleum Exploration and Production Research Institute, China
Tadeusz Peryt,
Polish Geological Institute, Poland

*CORRESPONDENCE
Ying Bai,
byshimmer@petrochina.com.cn
Zhenyu Zhao,
zhaozy01@petrochina.com.cn

SPECIALTY SECTION
This article was submitted to Sedimentology, Stratigraphy and Diagenesis, a section of the journal Frontiers in Earth Science

RECEIVED 07 November 2022
ACCEPTED 26 January 2023
PUBLISHED 08 February 2023

CITATION
Bai Y, Zhao Z, Zhao Z and Gao J (2023), Multiphase dolomitization mechanisms of the Cambrian upper Changping Formation, North China Platform, China. *Front. Earth Sci.* 11:1091424. doi: 10.3389/feart.2023.1091424

Multiphase dolomitization mechanisms of the Cambrian upper Changping Formation, North China Platform, China

Ying Bai*, Zhenyu Zhao*, Zhe Zhao and Jianrong Gao

Research Institute of Petroleum Exploration & Development, PetroChina, Beijing, China

The Cambrian dolomite reservoirs of the North China Platform offer good exploration prospects, but their occurrence and the impacts of dolomitization on reservoir quality are not yet clearly understood. The study herein assesses outcrop samples in the Cambrian upper Changping Formation, Dingjiatan area, and highlights the important role of multiphase dolomitization in the formation of paleo-reservoirs of acceptable porosity, where oil pools and fields may be discovered. A combination of petrology, fluid inclusion microthermometry, isotopes, and trace element compositions has been used to explain multiphase dolomitization mechanisms and their impacts on dolomite reservoirs. Five types of dolomites are identified through outcrop observation, thin section identification *via* transmitted light, and cathodoluminescence. The following geochemical analyses reveal various dolomitization mechanisms. In the (pene) contemporaneous stage, microbial dolomite is commonly related to microbial metabolic activities with significant carbon isotopic depletion compared to the Cambrian seawater values. With the influence of microbial dolomitization, dolomicrite corresponds to the sabkha dolomitization mode in a low-salinity seawater environment and early-stage dolomitization. The structureless dolomite (ssD) in the early highstand systems tract (EHST), characterized by elevated $^{87}Sr/^{88}Sr$ ratios and low oxygen isotopic values, forms from stratum brine water in the shallow-middle burial stage rather than in the (pene) contemporaneous stage. In contrast, ssD in the late highstand systems tract (LHST) undergoes (pene) contemporaneous dolomitization at salinities between 6% and 28% before later pore water transformation, with the participation of atmospheric freshwater through faults and unconformities exhibiting the lowest inclusion temperature and salinity values. The medium to coarse crystalline dolomite (MCD) in the LHST and the saddle dolomite (SD) in the EHST with low REE values are atypical hydrothermal dolomites caused by a combined superposition of middle-deep burial hydrothermal fluids at temperatures >150°C and stratigraphic brines. The MCD is also influenced by terrigenous water characterized by relatively low Eu anomaly values. Finally, the mechanisms of porosity increase are investigated, and it is concluded that the pore increase caused by the (pene) contemporaneous reflux interaction and the later pore retention both lead to better ssD reservoirs in the LHST than in the EHST.

KEYWORDS

dolomitization, Cambrian, Changping Formation, North China Platform, reservoir

1 Introduction

Recent exploration has proven that deep dolomite reservoirs usually offer great hydrocarbon potential (Azmy et al., 2001; Azmy et al., 2008; Jiang et al., 2014; Jiang et al., 2019; Liu et al., 2020; Zhemchugova et al., 2020). Therefore, the related dolomitization events and their various impacts on reservoir qualities have become the focus of research (Swart et al., 2005; Jiang et al., 2016; Jiang et al., 2019; Xu et al., 2021). Most representative ancient dolomite reservoirs associated with evaporite minerals originated from surface evaporitic seawater with high Mg/Ca ratios (Adams and Rhodes, 1960; Swart et al., 2005; Sumrall et al., 2015). At the same time, or earlier, microbial activities could potentially reduce the activation energy to form spherical and dumbbell-shaped dolomites in a low-temperature environment (You et al., 2011). Residual brines flow downwards after surface metasomatism and cause reflux dolomitization of the deep sediments and rocks sequentially along the flow path (Whitaker and Xiao, 2010). Affected by the Mg^{2+} supply and reduced activation at high temperatures, these deep reservoirs are continuously affected by burial and hydrothermal dolomitization during the burial diagenetic stage (Malone and Paul, 1996; Heydari, 1997; Davies and Smith, 2006). For example, Jiang et al. (2016) proposed that Cambrian microbial reservoirs in the Tarim Basin (China) reflect both microbial and sabkha dolomitization characteristics, and continuous reflux dolomitization has led to evaporitic dolomite with hydrothermal characteristics at depth.

Recent Cambrian exploration in the North China Platform has suggested great hydrocarbon prospecting, and only the potential of the Zhangxia Formation associated with palaeogeographic patterns and sedimentary distribution modes has been systematically reported in several contributions (Guo et al., 2018; Guo et al., 2019), revealing that various dolomitization events have caused difficulties in research and production. Thus, research on other Cambrian formations, such as the Changping Formation, and correlative dolomitization processes are still needed. Inspired by the exploration and development achievements of the Ordovician Majiagou Formation in the Ordos Basin, the Cambrian dolomite reservoirs have been attributed to a (pene) contemporaneous origin (Huang et al., 2016; Cui et al., 2018; Liu et al., 2021). However, it is difficult to apply the classic sabkha and reflux dolomitization modes in the Changping Formation with a lack of evaporite series (Adams and Rhodes, 1960), and the sealed burial systems obviously cannot provide sufficient fluids for large-scale dolomitization. Thus the dolomitization mechanisms of the Changping Formation need to be re-examined.

Here, new outcrop samples with an absence of evaporites were collected in the Dingjiatan area, and conventional specimen-description techniques, thin section identification, scanning electron microscope (SEM) petrography, fluid-inclusion studies and various isotopic analyses were used to explain the origins of different types of dolomite and relevant reservoir characteristics in the Lower Cambrian Changping Formation, North China Platform. Specifically, this study aims to determine the effects of multiphase dolomitization on reservoir properties and address the following three questions.

1) What are the representative petrological and geochemical characteristics of diverse dolomites?
2) What were the chief dolomitization mechanisms and diagenetic fluids?
3) How much do the different dolomitic interactions contribute to the formation of high-quality reservoirs?

2 Geologic setting

The North China Platform contains most of northern China and occupies an area of approximately 1.5 million km^2 (Figure 1A) (Hong et al., 2003; Cui et al., 2018). Under a warm, humid climate, the Lower Cambrian Changping Formation (in some areas known as the Fujunshan or Xinji Formations) was deposited in a tidal-dominated, epeiric sea and shallow marine complex after a significant sedimentation interruption of nearly 400 million years (Figure 1B) (Mei et al., 2011). It lies roughly in the lower fourth stage of the Cambrian second series, with a basal age of approximately 515 Ma, while that of the top boundary is more divergent, chiefly yielding an age of approximately 509 Ma (Mei et al., 2011; Bai et al., 2019; Bai et al., 2021b). These uncertainties are mainly due to a lack of isochronous trilobite biozones, which causes some difficulties in global correlation. Therefore, the Cambrian stratigraphic scheme in the North China Craton is mainly based on petrostratigraphy and sequence stratigraphy (Mei et al., 2011; Bai et al., 2019; Bai et al., 2021b).

The Dingjiatan area, located in the western suburb of Beijing, is mainly distributed in the Jizhong Depression, North China Platform (Figure 1A). In the study area, the Changping Formation is approximately 30 m thick and forms a three-order sequence (Figure 2A), comprising a transgressive systems tract (TST), an early highstand systems tract (EHST), and a late highstand systems tract (LHST). The TST is made up of the lower Changping Formation period, dominated by intertidal conglomerate and stromatolites (Figure 2A). This tract is mainly characterized by 1) widely distributed dark siliceous and argillaceous eluvial deposits, and 2) marked darkening of the sediments after the initial flooding (Figure 2B). The EHST and LHST sequentially overlie the TST with an overall thickness of approximately 20 m (Figures 2A, D). The EHST is dominated by a set of oncolite, thrombolite and stromatolite calcareous dolomites, which are composed of abundant sand, biogenic burrows and bioturbation structures (Figure 2C), indicative of a high-energy subtidal environment in the North China Block. Little lithological variation from south to north in the sections (Figure 3) represents vertical aggradation in the EHST. Compared with the EHST, the LHST features a thinner bed thickness (Figure 2D) and a higher degree of dolomitization, which are most likely representative of regression. The lithology varies from south to north and diminishes towards the south, showing characteristics of northward progradation in LHST (Figure 3) (Mei et al., 2011; Bai et al., 2019; Bai et al., 2021b).

The depositional period of the Changping Formation belongs to the Caledonian-Hercynian period, during which the plate activity in the Jizhong depression was calm but with oscillatory movements (Zhao et al., 2015; Yan, 2019). From the Mesozoic to Cenozoic era, three fracturing phases developed, facilitating the fluids to flow through the layers and modifying the reservoirs (Meng and Ming, 2003; Bai et al., 2019; Yan, 2019; Bai et al., 2021b).

The burial history shows that the eastern North China Platform underwent three subsidence phases (Feng et al., 1998; Zhao et al., 2015; Yan, 2019): 1) rapid subsidence from the Cambrian to the Ordovician; 2) slow uplift activities in the Hercynian period, followed by a brief subsidence period until the Triassic; and 3) a fluctuating subsidence phase after the Indochinese tectonic uplift. Additionally, two hydrocarbon charging events occurred in the Triassic and Paleogene as a result of fault transport. The former was mainly

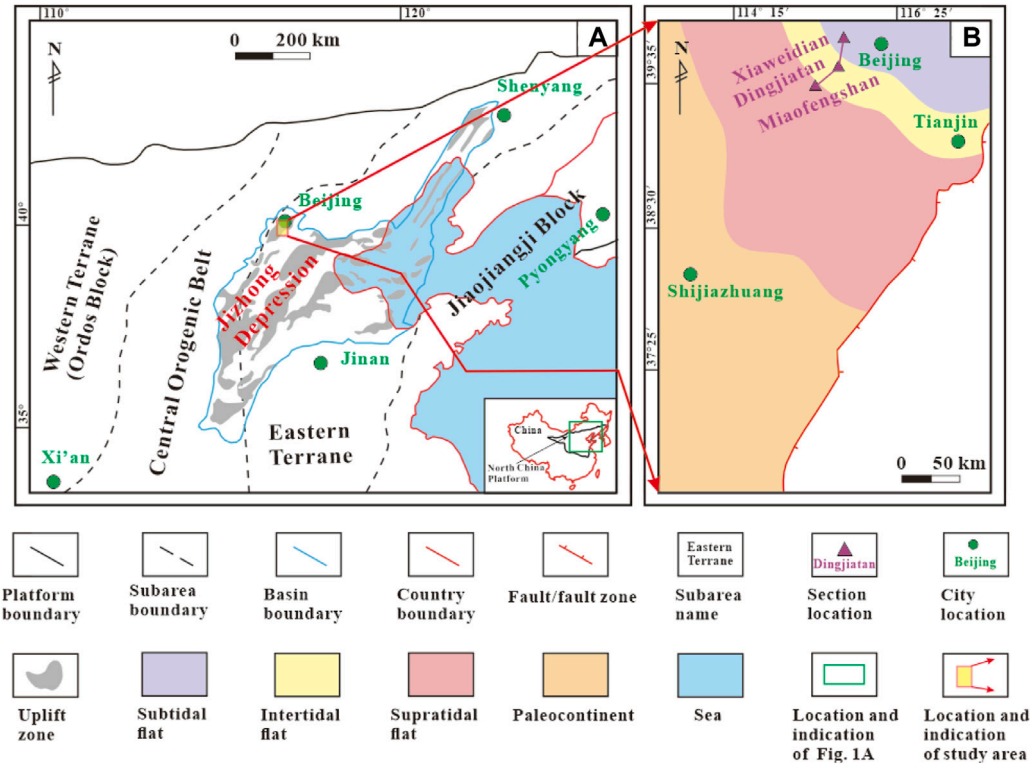

FIGURE 1
Map of the study area showing **(A)** an overview of the North China Platform and the location of the study area (adapted from Yu et al., 2022), and **(B)** the palaeogeography environment of the Cambrian Changping Formation and ths (adapted from Xiao, 2020).

derived from the Carboniferous-Permian coal-derived hydrocarbon rocks, and the latter from both secondary hydrocarbon generation and Paleoproterozoic argillaceous rocks.

3 Samples and methods

A total of 153 samples with intervals ranging from 0.1 to 1.0 m were collected from three outcrop sections that integrated the whole Changping Formation in the Dingjiatan area. After observing all hand specimens and corresponding thin sections, 48 representative upper Cambrian samples were used for detailed petrology and geochemistry research.

3.1 Petrological studies

Thin section and scanning electron microscope (SEM) images were obtained at the Petroleum Geology Experimental Research Center of the PetroChina Research Institute, Beijing. A Leica DMRX multifunctional microscope was used to analyse the transmitted light characteristics. Cathodoluminescence (CL) images were observed *via* a CITL CL8200 MK^5 CL microscope with an acceleration voltage of 15 kV and a beam current of 320 μA. A TESCAN VEGA II LMU SEM equipped with an energy dispersive spectrometer analysed the ultramicro component and element composition.

3.2 X-ray diffraction (XRD) order analysis

The X-ray diffraction order analysis was performed using a PANalytical X' multifunctional X-ray powder diffractometer with a voltage of 40 kV, a beam current of 40 mA, and measurement angles of 5°–70°. These analyses were conducted at ALS Analytical Chemistry and Testing Services, Guangzhou.

3.3 Fluid inclusion assemblage (FIA) observation and measurement

Polished sheets were carefully identified under transmitted and fluorescent light using a dual-channel Nikon 80I microscope with a Linkam THMS600 geology stage at the Beijing Research Institute of Uranium Geology. The detection limit of the two-phase inclusion size was >1 μm. The last ice melting and homogenization temperatures (T_h) were measured at a testing temperature of 25°C and humidity of 40%. The thermometry error was ±0.1°C, and salinity values (equivalent to wt% NaCl) were calculated by the ice-melting temperature conversion of standard equations (Bodnar, 2003).

3.4 Isotope analysis

Corresponding samples were ground into powder for stable oxygen and carbon isotope measurements. Each heated sample was

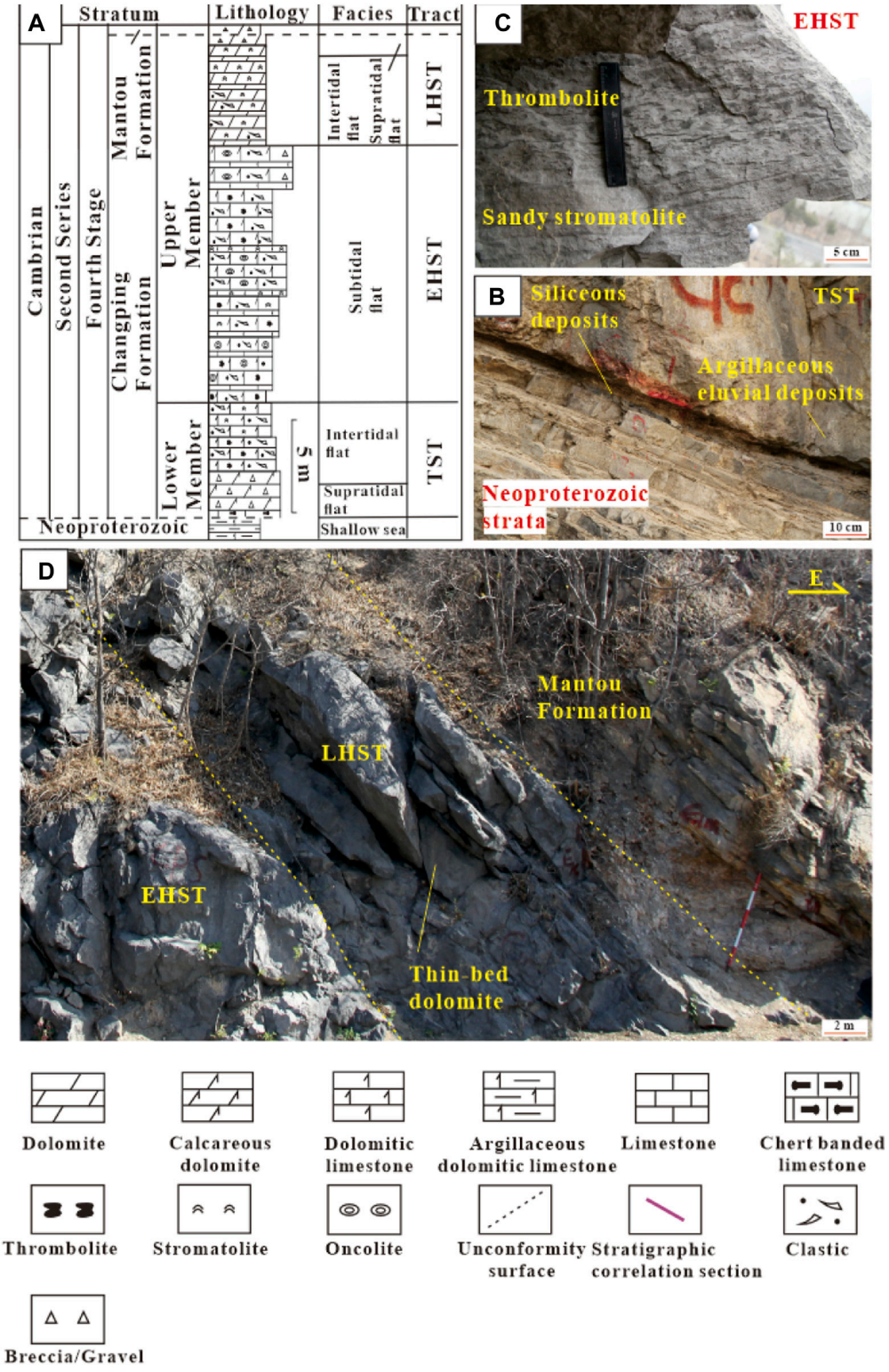

FIGURE 2
Stratigraphic characteristics of the Cambrian Changping Formation in the study area. **(A)** Comprehensive stratigraphic column of the Changping Formation (after Bai et al., 2019; Bai et al., 2021b). **(B)** Siliceous and argillaceous eluvial deposits in the TST, Dingjiatan section. **(C)**Sandy stromatolite and thrombolite in the EHST, Dingjiatan section. **(D)** Thin-bed dolomite in the LHST, Dingjiatan section.

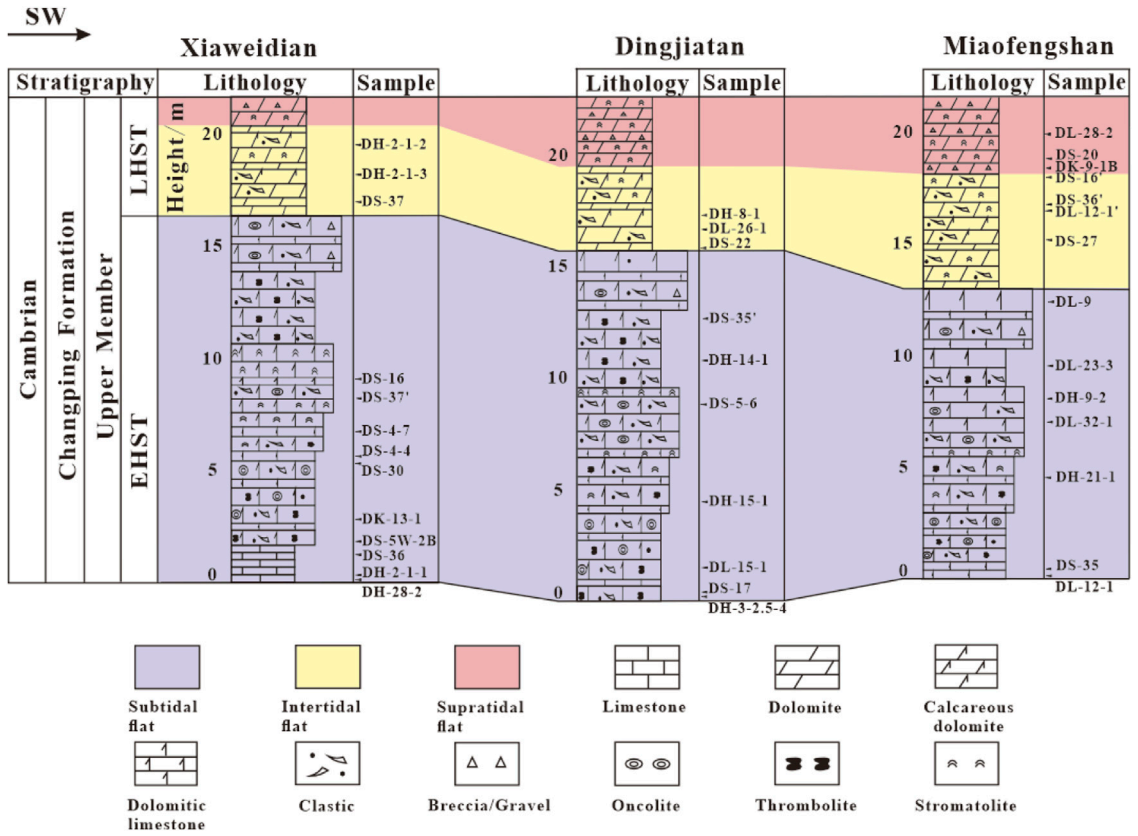

FIGURE 3
Outcrop-tie section (location shown in Figure 1B) exhibiting little lithological variation in the EHST, and various lithofacies in the LHST.

reacted with anhydrous phosphoric acid at 25°C for 24 h to release CO_2. The CO_2 was collected for analysis on a Finnigan MAT251 gas isotope mass spectrometer, and final data were reported following the Vienna Pee Dee Belemnite (VPDB) standard (Sauer et al., 2001), with a precision better than ±0.01%.

Strontium isotope ratio experiments were prepared by dissolving powder samples in ultra-pure acid at 60°C for 24 h. Separated strontium samples were used to measure ratios through a thermal ionization mass spectrometer (GV IsoProbe-T) and normalized to an NBS-987 ratio of 0.710253. The accuracies were better than 3×10^{-6}.

Magnesium isotope analysis included sample decomposition with acid and alkali dissolution methods and separation and purification using a cation exchange column. The main instrument was a Neptune multiple-collector inductively coupled plasma mass spectrometer with a relative standard deviation of <0.01%. The standard sample was a pure magnesium solution from Dead Sea Magnesium Ltd., Israel (DSM3) (Galy et al., 2003).

The above isotopic studies were all carried out at ALS Analytical Chemistry and Testing Services, Guangzhou.

4 Results

4.1 Petrography

The upper Cambrian Changping Formation in the North China Platform features different dolomitization degrees. The EHST has lower dolomitization degrees, and the LHST has higher degrees. Based on the dolomite observation results of macroscopic characteristics and microscopic morphologies, five dolomites were identified: dolomicrite (DM), microbial dolomite (mD), structureless dolomite (ssD), medium to coarse crystalline dolomite (MCD), and saddle dolomite (SD) (Figure 4; Supplementary Appendix S1).

4.1.1 DM

DM is commonly present throughout the upper Changping Formation and consists of muddy (mostly approximately 10 μm crystals) and generally non-planar-anhedral (nP-A) dolomite (Figure 4A). It commonly consists of light grey, parallel laminated beds, sometimes with massive structure. These DM samples have a red to dark red CL colour (Figure 4B) and low degrees of order (between 0.47 and 0.62, shown in Supplementary Appendix S1), indicating rapid crystal growth from the intertidal and subtidal zones (Goldsmith and Graf, 1958; Hood and Wallace, 2015). Spherical dolomite is observed (Figure 4C), commonly associated with mD or ssD of microbial-like textures in the EHST (Figure 4D), representing microbial induction (You et al., 2011).

4.1.2 mD

mD is mainly represented by the EHST, with low abundance in the LHST. It consists of very fine crystalline (mostly 10–20 μm crystals) and mostly nP-A to planar-euhedral (P-E) dolomite (Figure 4E). Sedimentary structures are well-preserved in mD, such as unattached spherical structures in oncolites (Figure 4D), laminated structures in

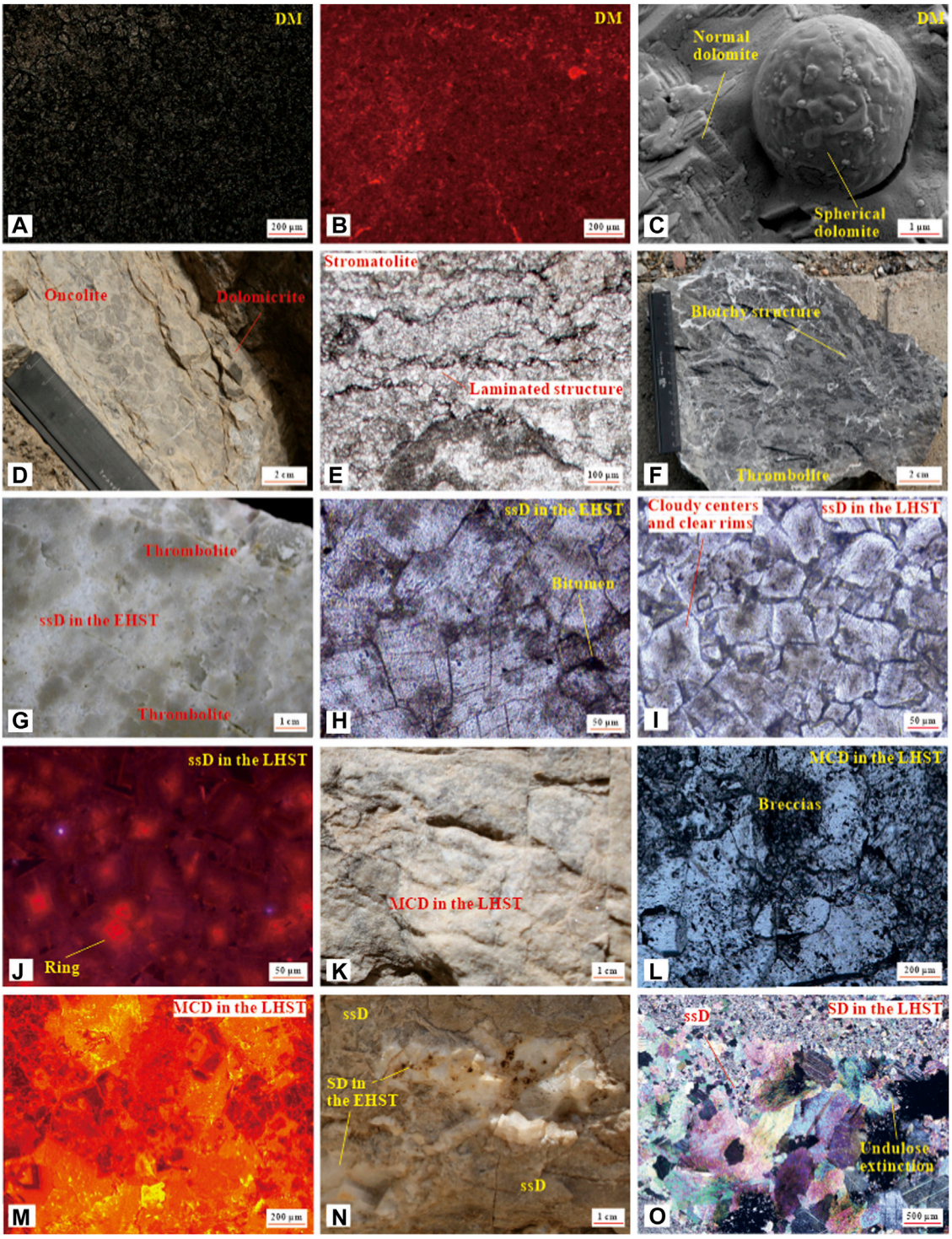

FIGURE 4
Petrological characteristics of the upper changping formation. **(A–B)** Plane-polarized light/CL image, DM, microcrystalline structure, dark red CL. **(C)** SEM image, spherical and normal rhombic dolomite. The samples shown in **(A–C)** are from 1.2 m in EHST, Xiaweidian Section. **(D)** Outcrop image, oncolites of unattached spherical structure associated with DM, 1.5 m in EHST, Dingjiatan Section. **(E)** Plane-polarized light image, stromatolite of laminated structure, 18.8 m in LHST, Miaofengshan Section. **(F)** Hand specimen photograph, thrombolite of blotchy structure, 2.5 m in EHST, Dingjiatan Section. **(G)** Polished hand specimen photograph, ssD of unclear original structure accompanied with thrombolite. **(H)** Plane-polarized light image, ssD of obliterative texture. Samples shown in panels **(I–J)** are from 7.0 m in EHST, Miaofengshan Section. **(I–J)** Plane-polarized light/CL image, ssD, foggy centres and clear rims, or ring effects. Samples shown in panels **(I–J)** are from 16.7 m in LHST, Dingjiatan Section. **(K)** Outcrop image, MCD in light grey to milky white. **(L–M)** Plane-polarized light/CL image, MCD in the LHST. The Samples shown in panels **(K–M)** are from 19.8 m in LHST, Miaofengshan Section. **(N)** Outcrop image, SD in milky white associated with ssD near the fault. **(O)** Cross-polarized image, SD, mosaic contacts and wavy extinction. Samples shown in panels **(N–O)** are from 6.7 m in EHST, Xiaweidian Section.

stromatolites (Figure 4E), and blotchy structures in thrombolites (Figure 4F). The mD exhibits a CL colour similar to that of DM, and a narrowly distributed degree of order, varying from 0.50 to 0.55 (Supplementary Appendix S1), indicates an irregular Mg^{2+} arrangement in the crystal lattice influenced by microbial metabolism (You et al., 2011; Baniak et al., 2014).

4.1.3 ssD

ssD primarily occurs in the whole upper Changping Formation. In the EHST, the degree of dolomitization is lower, about 30%, and the ssD can account for about 70% of the EHST dolomite. While in the LHST, the degree of dolomitization can be as high as 70%, and 80% of the dolomite can be ssD.

In the EHST, ssD and mD are in gradual contact (Figure 4G) on the hand specimen, and the fine to medium crystalline (mostly approximately 50 μm crystals), P-E and planar-subhedral (P-S) ssD display massive structures and obliterative microbial-like textures (Figure 4H). This blurred-ring dolomite has a dark red CL and medium-to high-order degree values with a narrow distribution (approximately 0.69–0.78, shown in Supplementary Appendix S1).

In the LHST, ssD features a foggy centre and bright edge (Figure 4I). Its noticeable ring effect occurs as an orange-red CL colour (Figure 4J), and the degree of order is widely distributed and high (approximately 0.75–0.89, shown in Supplementary Appendix S1). These two sets of high values may indicate lattice structure adjustment during the burial period (Machel, 2014), yet different zonal characteristics in CL images reveal distinct dolomitization processes in the upper Changping Formation.

4.1.4 MCD

MCD displays massive and saccharoidal structures and light grey to milky white colouration in the specimen (Figure 4K), and is primarily present in the LHST, particularly near the top karst surface with breccias (Figure 4L), but is not associated with the spatial distribution of fault locations. These well-developed paragenetic breccias suggest the impact of atmospheric water. Microscopically, MCD consists of medium to coarse crystalline, P-S, and nP-A dolomites, whose sizes range between 50 and 300 μm (Figure 4L), with bright red colour and an even bright red and yellow colour under CL (Figure 4M). A high degree of order, widely varying from 0.76 to 0.91 (Supplementary Appendix S1), corresponds to multiple adjustments of dolomitization (Jiang et al., 2016; Bai et al., 2021a).

4.1.5 SD

Milky white, structureless SD is mainly observed in the vicinity of fractures in the EHST, outside of which SD coexists with nearby ssD (Figure 4N). SD comprises coarse crystalline, nP-A dolomite (crystal diameters ranging from 300 to 1,500 μm), and mostly undulose extinction (Figure 4O), and shares a similar CL colour with MCD. The degree of order is widely distributed with high values (approximately 0.61–0.79) (Supplementary Appendix S1), which may imply incomplete and rapid dolomitization (Huang et al., 2006; Machel, 2014; Bai et al., 2021a).

4.2 Geochemical data

4.2.1 Fluid inclusion studies

Fluid inclusions are commonly used for dolomitization fluid property analysis, and FIAs have been defined following the rules of Goldstein and Reynolds (Goldstein and Reynolds, 1994). More than 90% of FIAs homogenization temperature (T_h) data from a given paragenetic type of mineral fall within a range of less than 10%–15%. Therefore, it is unlikely that thermal re-equilibration has occurred (Goldstein and Reynolds, 1994).

The results show that only aqueous single-phase saltwater inclusions approximately 2 μm in diameter are observed in DM and mD. This means that the formation temperature was lower than 50°C (Goldstein and Reynolds, 1994; Jiang et al., 2016). Fewer pure liquid inclusions are found in the EHST ssD than in the LHST ssD, probably suggesting less surface seawater dolomitization transformation in the EHST. These samples have narrow, bimodal T_h ranges of 60°C–80°C and 100°C–120°C near the faults (Figure 5A). Correspondingly, salinity data of the normal ssD derived from ice-melting temperatures are predominantly between 8 and 18 wt%. Under the influence of fault fluids, the salinity can reach approximately 14–32 wt% (Figure 5B). Many two-phase, liquid–gas inclusions are observed in the LHST ssD, showing an equally low and narrow T_h range from 60°C to 80°C, with a lower salinity range from 6% to 20%. The ssD approaching the faults grew at higher temperatures and salinities (approximately 90°C–120°C and 14 to 28 wt%). A few LHST samples near the top show the effect of freshwater, with T_h and salinity values of approximately 60°C–70°C and 6 to 8 wt%, respectively (Figures 5A, B). The SD values range from about 100°C to 200°C, and have relatively high salinities of approximately 14–30 wt%. However, the T_h (80°C–180°C) and salinity data (8–24 wt%) of the MCD samples both have wide ranges (Figures 5A, B), mainly indicating multiple fluids in the dolomitization process.

Two phases of oil and gas inclusions can be identified. Phase I is mainly developed in the LHST ssD (frequency of oil inclusions = 5%, hereafter FOI), whose inclusion component is mainly bitumen (Figure 5C), and phase II in SD and EHST ssD is associated with calcite (FOI = 8%), dominated by bitumen and CH_4 inclusions (Figure 5D). Distinct inclusion characteristics correspond to the dual hydrocarbon discharge events described previously.

The ground temperature gradient in the study area is 25°C/km, and the surface temperature is 20°C (Yan, 2019). Combining the homogeneous temperature and salinity, the capture depth and dolomite formation time are determined, with two accumulation events separating the overall burial history into three phases: 1) DM and mD have burial depths <1,200 m and were formed approximately during the (pene) contemporaneous period. 2) ssD has formation depths of 1,600–2,400 m and may have originated from moderate salinity fluids in the shallow-middle burial period. 3) The burial depths of MCD and SD are 2,400–6,400 m and 3,200–7,200 m, respectively, countering the middle-deep burial period. The "broad-peaked" temperature and salinity of MCD may indicate the influence of a wide range of fluids with different properties.

4.2.2 Rare earth element (REE) characteristics

REE parameters and patterns have good referential significance for dolomitization fluid determination (Bau and Dulski, 1965; Brand and Veizer, 1980; Bau, 1991; Muhammad et al., 2020); for example, δCe and δEu values can be used to distinguish seawater from meteoric water and a low-temperature dolomitization environment from a high-temperature environment (Banner et al., 1998; Bau and Alexander, 2006). Here, the REE distribution relationships and other correlative contents of dolostone, including

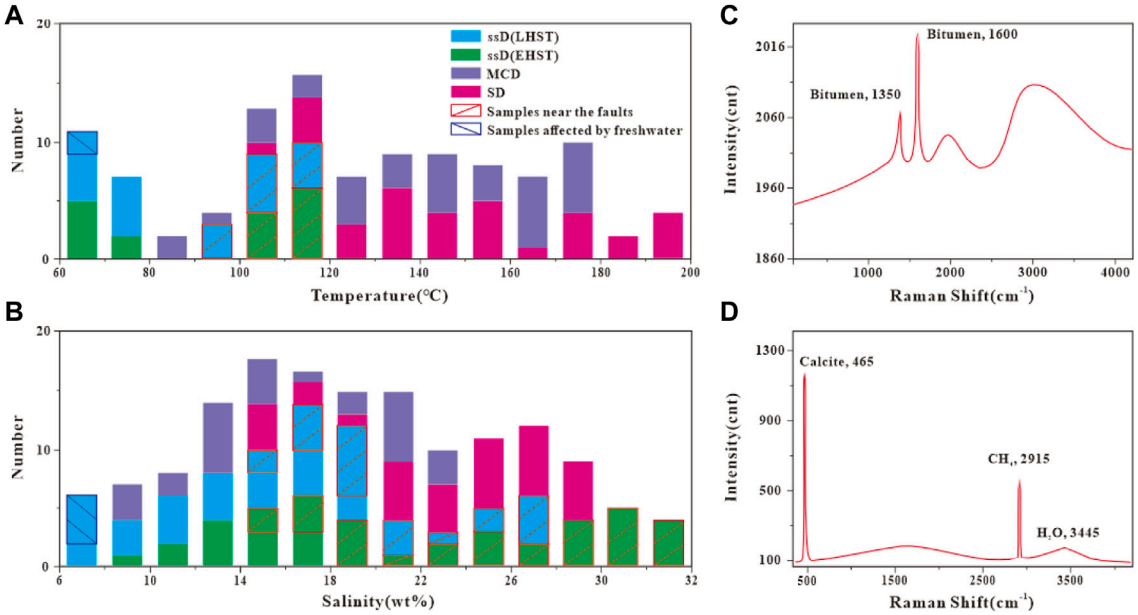

FIGURE 5
Homogenization temperature measurements and salinity determinations of inclusions in the investigated upper changping formation. **(A)** Homogenization temperature measurement results; **(B)** salinity determination results; **(C)** Raman spectrum characteristic of phase I hydrocarbon inclusions, mainly bitumen; **(D)** Raman spectrum characteristic of phase II hydrocarbon inclusions, chiefly CH_4.

associated limestone, were analysed (Figure 6; Supplementary Appendix S2). The analysis shows that all the limestone, DM, and mD exhibit nearly flat distribution characteristics of light REE (LREE) enrichment and heavy REE (HREE) loss (Figure 6A). Correspondingly, negative anomalies of δCe and δEu (<1) both indicate that those samples are mainly of seawater origin (Supplementary Appendix S2) (Azmy et al., 2011).

Some ssDs in the EHST display characteristic left-leaning patterns and are typical of seawater genesis (Kawabe et al., 1998) (Figure 6B). Samples associated with fractures and veins have δEu values greater than 1.15 (Supplementary Appendix S2). Because Eu^{2+} can enter lattices affected by hydrothermal fluids and replace internal Ca^{2+}, Eu features a positive anomaly (>1) in such circumstances (Alibo and Nozaki, 1999; Kucera et al., 2009; Swart, 2015). Therefore, these data suggest a representative hydrothermal environment.

The ssD in LHST exhibits a similar distribution pattern compared to the marine carbonates (Figure 6B). However, compared to the EHST samples, the LHST samples show a reduced enrichment in LREEs and an increased enrichment in HREEs. In addition, the ssD in the vicinity of hydrothermal-genetic veins has a low positive anomaly of less than 1.1 (Supplementary Appendix S2). Therefore, this type of dolomite may have been modified by fluids other than seawater and hydrothermal liquids (Morad, 1998; Morad et al., 2010). Three Ce anomalous samples, including DH-8-1, DL-26–1, and DS-22, are identified (Supplementary Appendix S2). They have δCe values slightly greater than 1, which may indicate the influence of atmospheric freshwater (Kucera et al., 2009; Swart, 2015). The remaining two samples, which are far from the fault and unmodified by hydrothermal fluids and freshwater, have high overall REE contents (Supplementary Appendix S2) (Haas et al., 1995; Friedman, 2007; Morad et al., 2010; Azmy et al., 2011; Kareem et al., 2021).

MCD and SD are common hydrothermal dolomite crystal forms in petrology, yet atypical REE characteristics (Figure 6C) shed light on the lack of associated hydrothermal minerals (Figures 3, 4) (Shields and Stille, 2001). Their flat REE distribution patterns are similar to those of limestone, indicating the effective influence of seawater-related diagenetic fluids. Even though Eu in some samples shows different degrees of enrichment, compared with typical magmatic rock values (mainly w (Sc) ≈ (5–10) × 10^{-6}; w (Th) ≈ (2–50) × 10^{-6}; w (Hf) ≈ (2–5) × 10^{-6}; and w (Zr) ≈ (50–200) × 10^{-6}, given in Budd, 1997; Huang, 2014; Hao et al., 2020), crustal elements are always present at less than 1.00 × 10^{-6}. Only one MCD sample has a Th value of 2.77 × 10^{-6}, which is in the normal range (Supplementary Appendix S2). As this sample is close to the unconformity and has the highest REE values among all the samples, the influence of terrigenous material and atmospheric freshwater on REE values should not be ignored, which could explain the relatively low Eu anomaly values in the MCD compared to the SD in the lower strata (Supplementary Appendix S2). However, we do not observe positive Ce anomalies in these atypical hydrothermal dolomites, unlike in the ssD, which may indicate that the hydrothermal concentrations can mask the presence of meteoric water.

4.2.3 Major and trace element characteristics

The relative contents of the major compounds MgO and CaO are effective parameters used to assess the dolomitization mechanism and degree of metasomatism (Zhao and Jones, 2012a; b). The results (Figure 7A; Supplementary Appendix S3) show that the ratios of MgO/CaO in DM and mD are primarily concentrated between 0.665 and 0.710, close to those in theoretical dolomite, $CaMg(CO_3)_2$ (0.714, according to Qian et al., 2019). Some DM samples were affected by terrigenous components, and their ratios reached 0.728. As shown in Figure 7A, DM and mD mainly feature

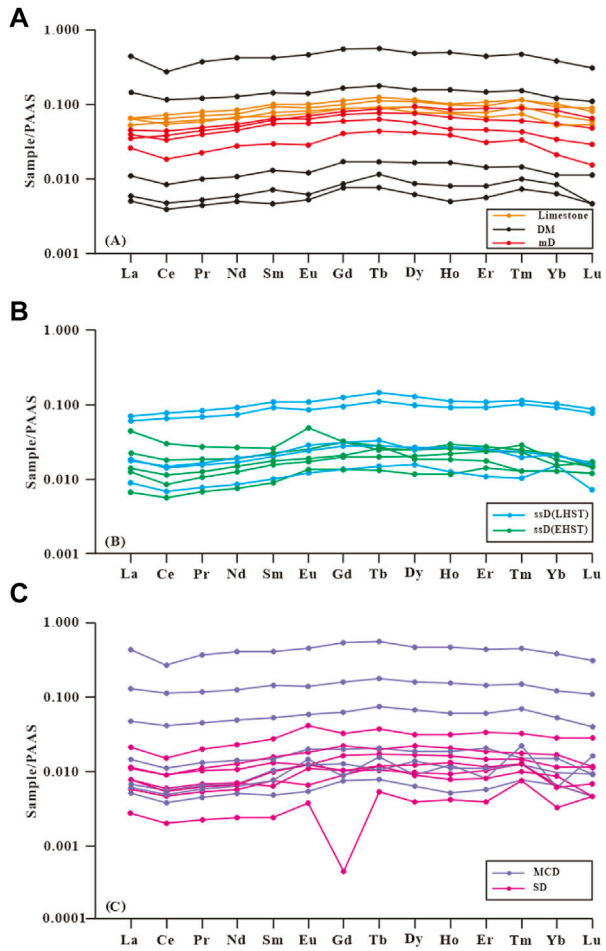

FIGURE 6
Distribution patterns of REEs in the investigated changping formation. **(A)** REE characteristics of limestone, DM and mD; **(B)** REE characteristics of ssD in the LHST and EHST; **(C)** REE characteristics of MCD and SD.

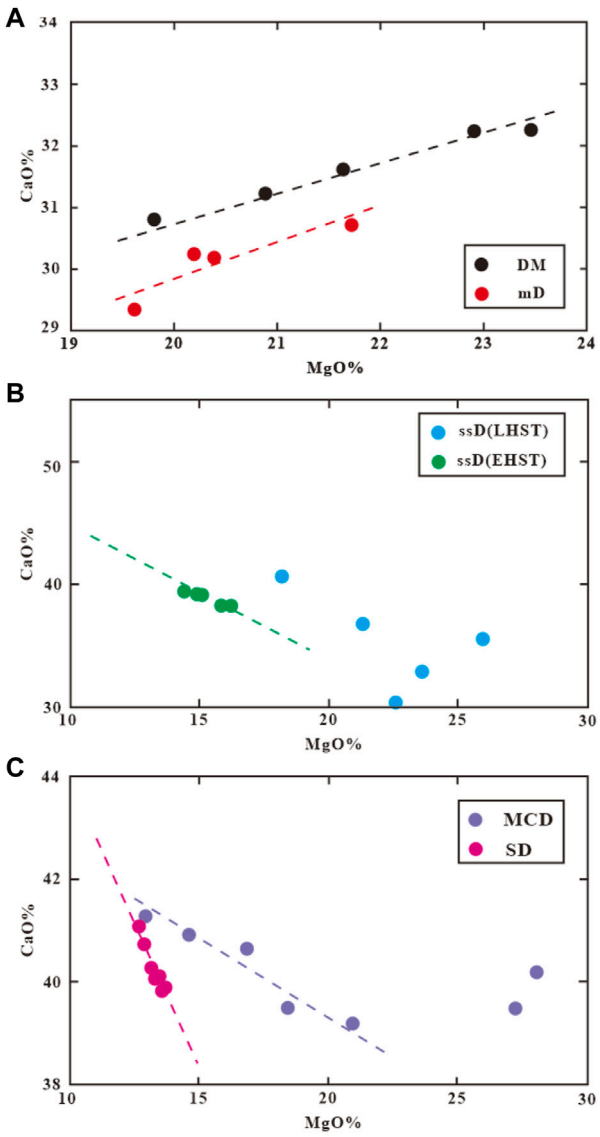

FIGURE 7
MgO and CaO crossplot of the upper changping formation. **(A)** MgO and CaO characteristics of DM and mD; **(B)** MgO and CaO characteristics of ssD in the LHST and EHST; **(C)** MgO and CaO characteristics of MCD and SD.

typical positive correlations, indicating that Ca^{2+} and Mg^{2+} can be added into the dolomite lattice synchronously. This feature is typical of (pene) contemporaneous dolomitization in an open environment (Kırmacıa et al., 2018).

The ssD ratios in the EHST are lower than 0.400 (Figure 7B; Supplementary Appendix S3), which, combined with the overall low degree of dolomitization in this tract, suggests inadequate dolomitized fluids. Correspondingly, the negative MgO-CaO correlation indicates that as the process of dolomitization progresses, the amount of Mg^{2+} in the diagenetic environment gradually decreases and, therefore, produces restricted dolomitization conditions (Kaczmarek and Sibley, 2011). The ssD ratios in the LHST have a wide range from 0.446 to 0.720 (Figure 7B; Supplementary Appendix S3), probably representing a rock-forming environment between closed and open conditions. These ratio values are mainly arranged in a dual-correlated manner (Figure 7B), indicating multiple dolomitized settings.

SD yields lower values (mainly <0.35), and the correlation is strong but negative (Figure 7C; Supplementary Appendix S3). These values suggest limited Ca^{2+} supplements in a restricted burial environment (Vahrenkamp and Swart, 1990). The MgO/CaO ratios of MCD feature a broad peak characteristic (0.239–0.698) (Supplementary Appendix S3). The low values rank negatively (Figure 7C), indicative of a confined diagenetic environment. Two points of high values (>0.60) are evidence of open dolomitization conditions with sufficient fluid exchange transformed by faults and cracks (Tortola et al., 2020).

Trace elements Fe and Mn are sensitive to fluctuations in the dolomitization environment because these two elements are more likely to enter the dolomite lattice than Sr and Ba in the buried environment, which can reflect higher values in the buried dolomite than in the oxidized, (pene) contemporaneous dolomite (Hiatt and Pufahl, 2014; Huang, 2014). A relatively strong regularity can be observed in Supplementary Appendix S3, where the DMs and mDs yield minimal Fe and Mn values down to approximately 400 and 40 on average, indicating near-surface oxidation

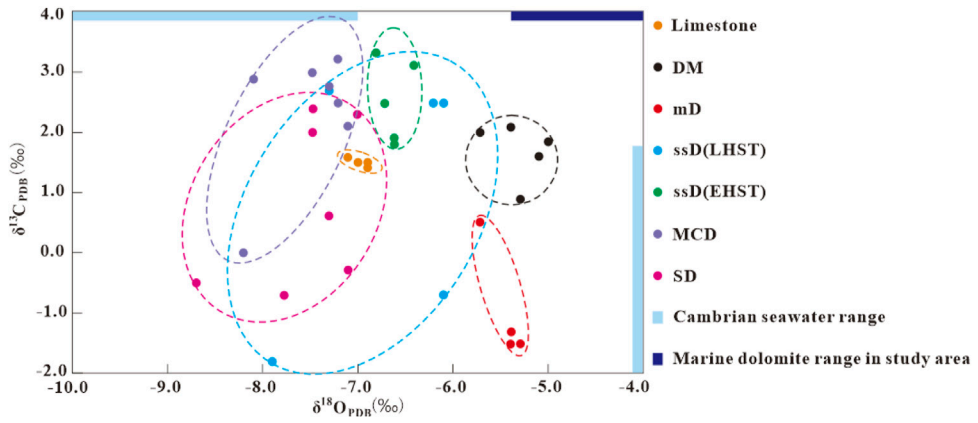

FIGURE 8
Carbon and oxygen isotopic crossplot of the upper changping formation.

dolomitization (Al-Aasm, 2000; Al-Aasm and Crowe, 2018). Notably, diagenesis related to the weathering crust has increased the values of nearby samples.

The ssD values are moderate and have a wide range, showing the transitional formation (Supplementary Appendix S3). The MCD and SD display relatively broad values of multiple dolomitization effects, with Fe contents ranging between 500 and 1700 and Mn contents ranging between 12 and 162, respectively (Supplementary Appendix S3). However, Fe and Mn values of some samples are significantly lower than those of other buried dolomites (mostly Fe > 1,000 μg/g, Mn > 100 μg/g, Budd, 1997). In addition, strongly reduced burial dolomitization is indicated only when Fe >1,000 μg/g and Mn > 10–100 μg/g. Therefore, MCD and SD are not totally derived from typical burial diagenesis (Budd, 1997; Hiatt and Pufahl, 2014).

4.2.4 Carbon and oxygen isotopic analyses

Stable carbon and oxygen isotopes are commonly used as indicators of palaeo-oceanic environments, rock-formation intensity analysis, and tracers of carbonate fluid origins (Carpenter et al., 1991). The carbon and oxygen isotopes in limestone samples display a relatively narrow range of values, namely, between 1.3‰ and 1.6‰ for $\delta^{13}C$ and between −6.9‰ and −7.1‰ for $\delta^{18}O$, which are largely within the scope of contemporaneous Cambrian seawater calcite (approximately −2.7‰ < $\delta^{13}C$ < 1.6‰ and −7.0 < $\delta^{18}O$ < −10.0‰, according to Huang, 2014; William, 1989) (Figure 8; Supplementary Appendix S4).

On the basis that the $\delta^{18}O_{PDB}$ value of seawater dolomite is 1.5‰ ~ 3.5‰ higher than that of calcite (William, 1989; Huang, 2014), the $\delta^{18}O$ value of marine dolomite in the upper Changping Formation should be between −5.4‰ and −3.6‰ (Figure 8; Supplementary Appendix S4). With this reference, we explore the fluid characteristics of various dolomites.

The DM and mD values are mainly within the range of those of contemporaneous seawater dolomite. Some DM values are close to the mD values, implying genesis similarities during the (pene) contemporaneous period. Microbial metabolism and methane oxidation can cause a decrease in $\delta^{13}C$ values (Jiang et al., 2016; Jiang et al., 2019), e.g., $\delta^{13}C$ values for DM can be concentrated at approximately 1.8‰, while those of mD are as low as approximately −1.5‰ (Figure 8; Supplementary Appendix S4).

The ssD of the EHST and LHST show distinct differences in carbon and oxygen isotopes. The narrow range of EHST samples reflects simple diagenesis. Its overall extent is closer to that of the limestone than to those of the DM and mD. This pattern may indicate that the less dolomitized EHST stratum has retained seawater-forming limestone features. Such low values of oxygen isotopes could also reflect burial genesis. The ssD of the LHST, with its wide range of carbon and oxygen isotopes, may indicate multiple geneses (Figure 8; Supplementary Appendix S4).

The $\delta^{18}O$ values for the MCD and SD are similar to those of seawater, suggesting that they were influenced by residual seawater. However, the $\delta^{13}C$ values for some MCD and SD are significantly positive, essentially above 2.0–2.5‰ (Figure 8; Supplementary Appendix S4). This is because high-temperature hydrothermal fluids could cause low oxygen contents in seawater, leading to increased carbon burial rates and consequently high $\delta^{13}C$ values (Ahmad et al., 2021; Mansurbeg et al., 2021).

The Keith & Weber salinity index formula, $Z = 2.048\ (\delta^{13}C + 50) + 0.498\ (\delta^{13}O + 50)$, has been applied mainly to identify the salinity of dolomitization fluids (generally Z > 120 for seawater diagenesis and Z < 120 for freshwater diagenesis) (Keith and Weber, 1964). Combined with the $\delta^{13}C$ and $\delta^{18}O$ values, it is suggested that mD was basically formed in a typical seawater environment, and its Z value is mainly stable at approximately 120. This result illustrates that microorganisms can form dolomite in a normal seawater environment. DM is likely influenced by both regular and saline seawater, with Z values between 127 and 129 (Supplementary Appendix S4).

Excluding the effect of hydrothermal fluids, the EHST ssD, which retains the characteristics of seawater, has the highest Z values between 129 and 131, demonstrating the presence of concentrated brine during the burial period. Some of the values of LHST ssD samples near the stratigraphic interface are below 120, showing freshwater influence (Supplementary Appendix S4).

The MCD and SD have Z values as high as 130, indicating the interaction of high-salinity hydrothermal fluids with stratum brines. Sample DK-9-1B, which has values as low as 123, may have been affected by atmospheric freshwater (Supplementary Appendix S4).

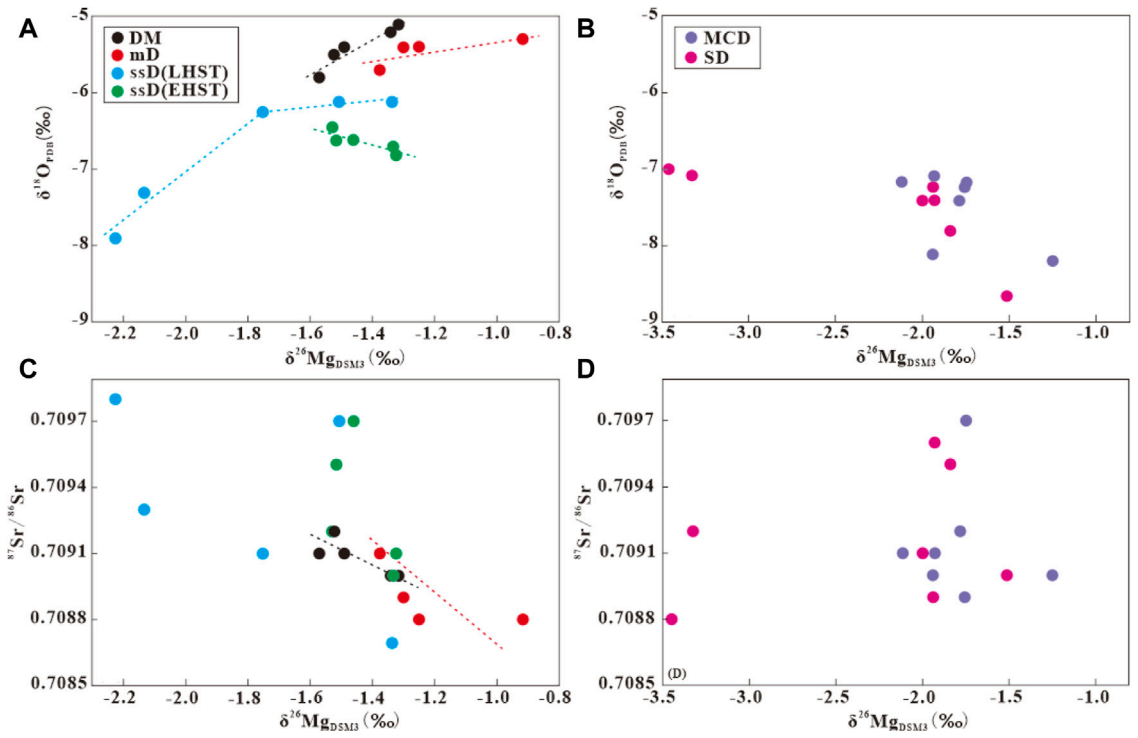

FIGURE 9
Isotopic crossplots of the upper changping formation. **(A)** Oxygen and magnesium isotopic crossplot of DM, mD, and ssD; **(B)** Strontium and magnesium crossplot of DM, mD, and ssD; **(C)** Oxygen and magnesium isotopic crossplot of MCD and SD; **(D)** Strontium and magnesium crossplot of MCD and SD.

4.2.5 Strontium and magnesium isotopic analyses

The composition of Sr isotopes in seawater is mainly controlled by terrestrial Sr-rich fluids and mantle-derived Sr-poor fluids and has been globally homogenized over a certain geological period (Burke et al., 1982; Denison et al., 1997). Because this fractionation is not affected by biology, salinity, temperature and pressure, the $^{87}Sr/^{86}Sr$ values may reflect dolomitization fluid properties and the environment (Burke et al., 1982; Denison et al., 1997). As shown in Supplementary Appendix S4, the $^{87}Sr/^{86}Sr$ values in the Changping Formation are largely within the range of Cambrian seawater (0.7087–0.7094, according to Burke et al., 1982; Huang, 2014), with a strong regularity, namely, mD < DM < MCD < SD < ssD (EHST) < ssD (LHST) (Supplementary Appendix S4), suggesting a gradual weakening of the influence of open seawater dolomitization systems (Burke et al., 1982; Carpenter et al., 1991). In addition, some ssD, MCD and SD samples have higher values with the influence of radioactive strontium in hydrothermal and Sr-rich atmospheric fluids (Figure 9; Supplementary Appendix S4).

Dolomite leads to higher $\delta^{26}Mg$ values (Mavromatis et al., 2013; Mavromatis et al., 2014), and its fractionation characteristics are mainly influenced by fluid properties, crystal size and crystallization order (Pogge von Strandmann, 2008; Pogge von Strandmann et al., 2008; Hippler et al., 2009; Schott et al., 2016). The mean values of $\delta^{26}Mg$ and crystal diameters are, respectively, ranked in the order of mD > ssD (EHST) > DM > MCD > ssD (LHST) > SD and SD > MCD > ssD (LHST) > ssD (EHST) > mD > DM (Supplementary Appendix S4), and the two factors are not strongly correlated. The preceding contents have shown that mD and DM crystallized the earliest, while MCD and SD crystallized the latest. This order does not correlate significantly with $\delta^{26}Mg$ values, so crystal sizes and crystallization order in the Changping Formation may not be the main factors influencing the values.

Compared to typical hydrothermal dolomites, the SD and MCD have higher $\delta^{26}Mg$ values ($\delta^{26}Mg < -2.0‰$, Tipper et al., 2006a; Tipper et al., 2006b). The MCD even shares similar values with the ssD of seawater genesis. Thus, $\delta^{26}Mg$-$\delta^{18}O$ and $\delta^{26}Mg$-$^{87}Sr/^{86}Sr$ covariograms were analysed to identify the dolomitization fluids (Figure 9).

Mg isotopes are not affected by temperature and salinity, and O isotope values are mostly proportional to salinity. Therefore, the positive correlation in the $\delta^{26}Mg$-$\delta^{18}O$ covariogram indicates that the enrichment of Mg isotope and Mg^{2+} synchronized with the dolomitization process is synchronized with the O isotope enrichment. In other words, Mg^{2+} is constantly trapped into the lattice as the diagenetic fluid is gradually concentrated. These characteristics reflect an abundant supply of Mg^{2+} in the diagenetic environment rather than the Mg^{2+}-limited closed environment. That is, Mg^{2+} may be essentially derived from evaporated seawater. Furthermore, both DM and mD have a positive correlation. Still, the slope of DM is steeper (Figure 9A), which may indicate that the salinity of the dolomitization fluid has a greater influence on DM formation, while mD may also have other more efficient mechanisms for low-salinity dolomitization. The $\delta^{26}Mg$-$^{87}Sr/^{86}Sr$ covariograms of DM and mD

also support this view from another perspective, as their negative correlations indicate simultaneous enrichment of Mg isotope and Mg^{2+}, and Sr depletion caused by the lighter mantle-derived strontium continuously trapped into the dolomite lattice. This evidence suggests that DM and mD originated from seawater. The mD slope is steeper (Figure 9B), which may indicate that more seawater is needed to obtain enough Mg^{2+} during the dolomitization process. This is related to the lower salinity of dolomitization fluid that formed mD.

The ssD values of EHST and LHST show different correlations in the $\delta^{26}Mg$-$\delta^{18}O$ plot (Figure 9A). The EHST samples with negative correlations reflect a buried dolomitization environment. The closed diagenetic system is unable to replenish Mg^{2+}, so as the brine continues to concentrate, increasingly less Mg^{2+} can enter the lattice (Heydari, 1997; Whitaker and Xiao, 2010). The Mg and Sr isotopes are not correlated (Figure 9B). This suggests fluid modification from various diagenetic environments. Combined with the C and O isotope and Z value signatures (Figure 8; Supplementary Appendix S4), the (pene) contemporaneous fluids might not cause dolomitization under open conditions, and dolomitization in the EHST ssD likely occurred only in the burial period and was accompanied by phase II hydrocarbon accumulation.

The LHST samples with two distinct slopes of positive $\delta^{26}Mg$-$\delta^{18}O$ relationships exhibit different dolomitization mechanisms in an open environment (Figure 9A). The higher slope values typically result from open (pene) contemporaneous dolomitization events. The samples with slope values of almost zero reflect continuous dolomitization at nearly constant salinity. These phenomena are indicative of outer freshwater injection preventing the continued concentration of stratigraphic brine in a confined environment. If attributed to terrigenous water alone, these samples probably pose a negative distribution in the $\delta^{26}Mg$-$^{87}Sr/^{86}Sr$ aspect, as terrestrial-derived Sr is heavier (Burke et al., 1982; Carpenter et al., 1991). However, the random distribution of LHST ssD samples in the $\delta^{26}Mg$-$^{87}Sr/^{86}Sr$ diagram presents multiple origins (Figure 9B). Therefore, the seawater might still be replenished during the dolomitization process, although it is likely to be highly saline.

The MCD and SD samples in the $\delta^{26}Mg$-$\delta^{18}O$ diagram display an obscure negative correlation (Figure 9C), which may indicate an unconfined diagenetic environment affected by fractures and unconformity surfaces. Thus, infiltrating seawater is still involved in the dolomitization process. Additionally, these samples are not correlated in the $\delta^{26}Mg$-$^{87}Sr/^{86}Sr$ plot (Figure 9D). Combining the results of ssD may reveal that strontium and magnesium isotope covariation graphs are not very sensitive to mixed-source dolomitization fluids.

Based on the above lithological features, the results of microtemperature measurements and relevant geochemical analyses, it is concluded that mD and DM are of (pene) contemporaneous marine origin. The EHST ssD has both (pene) contemporaneous diagenetic characteristics with shallow-medium burial dolomitization, but hydrothermal effects cannot be completely excluded. The LHST ssD is the dolomitization product of seawater, strata brine and atmospheric freshwater. The MCD and SD are of burial origin, with the former mainly consisting of strata brine, hydrothermal and atmospheric fluids, and the latter chiefly consisting of residual concentrated seawater and hydrothermal liquids.

5 Discussion

5.1 Dolomitization mechanisms for the changping formation in the north China platform

5.1.1 The (pene) contemporaneous microbial dolomitization mode

The Z values in Supplementary Appendix S4 show that mD can form in a typical seawater environment. Correspondingly, many single-phase inclusions in the Changping Formation indicate that they likely formed in a low-temperature surface environment rather than in a high-salinity burial environment (Jiang et al., 2016). This is because the extracellular polymeric substances produced from microorganisms can overcome the kinetic barriers posed by low-salinity seawater and increase the alkalinity of the local water environment, leading to dolomite supersaturation and ultimately to dolomite precipitation (Vasconcelos et al., 1995; Vasconcelos and McKenzie, 1997; Sumrall et al., 2015). Correspondingly, the negative carbon isotopic drift in mD (Figure 8) indicates vigorous metabolic activities (Jiang et al., 2016). Their REEs and major and trace elements (Figures 6, 7; Supplementary Appendixes S2, S3) reflect unrestricted environmental characteristics (Banner et al., 1998; Azmy et al., 2011). Associated values of oxygen isotopes are within the range of those of sea-derived dolomites (Figure 8), also suggesting that primary seawater may have been the main fluid for microbial dolomitization.

Microbial dolomitization also occurred in DM. Spherical and normal dolomites are observed in symbiosis (Figure 4C) and have geochemical indicators similar to those of mD (You et al., 2011). However, dolomicrite does not reach the level of microbialites, and the absence of a negative shift in carbon isotope values (Figure 8) implies a strong influence of (pene) contemporaneous sabkha dolomitization (Baniak et al., 2014; Ahmad et al., 2021).

5.1.2 The (pene)contemporaneous sabkha and reflux dolomitization mode

Early diagenetic gypsum is not observed in the Changping Formation, so in a strict sense, there is no typical sabkha environment in the Dingjiatan area (Mei, 2011; Bai et al., 2021b), i.e., mD and DM that formed in the near-surface and (pene) contemporaneous phases are also the products of low-salinity seawater (Figure 10A).

This phenomenon depends to some extent on microbial activity and induction, and on the other hand, research in recent years has suggested that low-salinity seawater can cause large-scale dolomitization (excluding microbial dolomitization) under early low-temperature conditions (Jones and Xiao, 2005). For example, for DM with open, sea-derived geochemistry, lithological characteristics demonstrate that microbial action does not have the capacity for large-scale dolomitization (Figure 4C; Figures 6–9; Supplementary Appendixes S2–S4). Note that compared to typical microbial dolomitization, products of sabkha dolomitization have a slightly higher Mg^{2+}/Ca^{2+} ratio (Figure 7; Supplementary Appendix S3) without reaching the salinity of gypsum precipitation, which may be related to frequent sea-level fluctuations in the early Cambrian North China Plateau (Mei, 2011). Reflux events are reflected in the fact that ssD retains the isotopic and REE information of seawater, and exhibits geochemical characteristics with a gradual increase in salinity (Figures 6–9; Supplementary Appendixes S2–S4). The carbon and

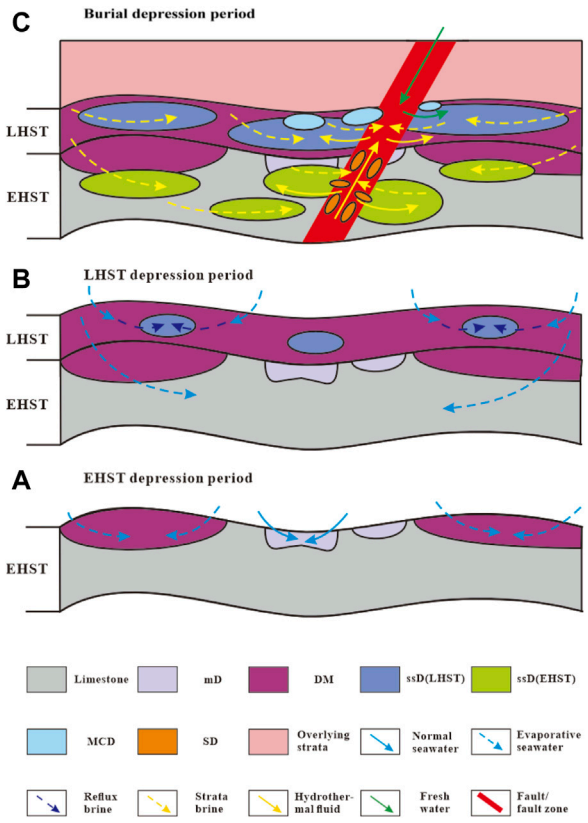

FIGURE 10
Multidolomitization process and mode in the upper changping formation. **(A)** EHST depression period; **(B)** LHST depression period; **(C)** Burial depression period.

oxygen isotopic ranges of ssD overlap with those of DM and mD and have lower oxygen isotope values (Figure 8), indicating that reflux is a continuation of sabkha evaporation near the surface. Lithologically, it is also acceptable that porous rocks in the high-energy zone can allow surface brine to pass through and penetrate deep into the strata (Hein et al., 1992; Jones and Xiao, 2005; Mahboubi et al., 2016), and the relevant evidence is that the LHST ssD shows zonal growth, with the earlier dolomite as a core (Figure 4I).

However, not all back-flow liquids can cause reflux dolomitization. The original rocks of the EHST ssD underwent (pene) contemporaneous transformation. However, the timing of effective dolomitization is within the shallow-medium burial period (Figures 10, 11). The lack of large-scale (pene) contemporaneous dolomitization is due to a high sea level and overall low evaporation in the EHST period. The resulting low salinity of the infiltrating seawater is not sufficient for reflux dolomitization to occur after surface dolomitization is completed. Additionally, the EHST has a low degree of dolomitization, indicating that (pene) contemporaneous sabkha and reflux phenomena both play important roles in large-scale dolomitization. By comparison, the overall drop in sea level during the LHST resulted in greater evaporation, causing brine downwelling and reflux dolomitization in LHST strata (Figure 10B).

5.1.3 The burial dolomitization in the shallow-middle burial period

Related studies in other basins have shown that (pene) contemporaneous infiltrated brine was continuously preserved in the formation and interacted with the surrounding strata during the shallow-middle burial period in a water-rock interaction (Jiang et al., 2016; Lukoczki et al., 2019), as evidenced by the dual isotopic geochemical characteristics of both evaporated seawater and burial

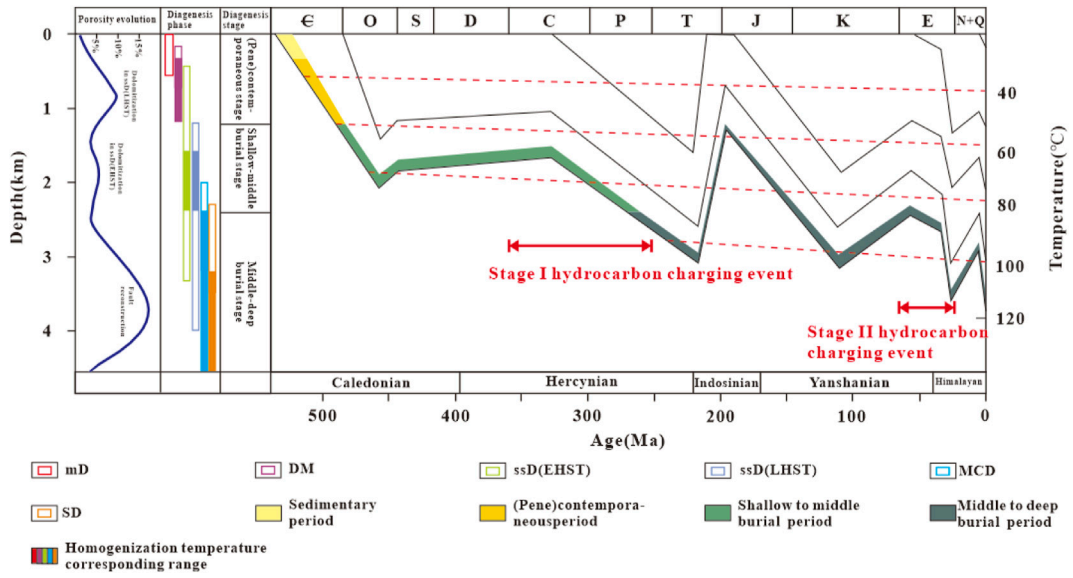

FIGURE 11
Burial and diagenetic evolution history in the upper changping formation, Dingjiatan area, North China platform.

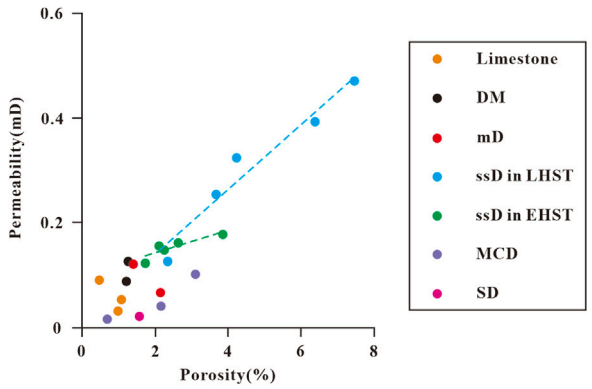

FIGURE 12
Crossplot of porosity and permeability in the upper changping formation, Dingjiatan area, North China Platform.

environment in the LHST ssD (Figures 7–10), which is a typical reflux product.

However, the EHST and LHST ssD samples show obvious differences. The LHST specimens have a broad range of MgO/CaO ratios (Figure 7B). The higher values of positive correlation reflect a (pene) contemporaneous open environment, while the lower values tend to be negatively correlated, indicating dolomite lattice adjustment during the shallow-middle burial stage. The high XRD data (Supplementary Appendix S1) with typical seawater isotopic information (Figures 5–9) also show pore water interactions following (pene) contemporaneous dolomitization, and atmospheric freshwater can also enter the LHST strata and participate in ssD (Figures 5, 9; Supplementary Appendixes S2–S4). In contrast, the EHST samples have only one set of negatively correlated low values, indicating that they represent the direct production of shallow to medium burial dolomitization. In other words, no (pene) contemporaneous dolomitization event occurred in the EHST ssD, as mentioned in chapter 5.1.2. These two types of burial dolomites are also present in the Lower Ordovician Penglaiba Formation in the Tarim Basin (Qiao et al., 2021).

5.1.4 The hydrothermal dolomitization in the middle-deep burial period

The burial history (Figure 11) shows that during the middle-deep burial phase, the Changping Formation was buried at depths up to 3,500 m and burial temperatures up to 120°C. Such conditions were favourable for hydrothermal dolomitization. The MCD and SD also show noticeable hydrothermal features of lithology (Figures 4K, 4N, 4O, 5) and geochemistry (Figures 8, 9).

However, the δ^{26}Mg values and crustal element contents of the MCD and SD differ significantly from those of typical hydrothermal rocks (Figure 9; Supplementary Appendixes S2–S4), and the Fe and Mn contents indicate that they are also not typical burial products (Supplementary Appendix S3), while the REEs are instead characteristic of seawater geochemistry (Supplementary Appendix S2). These results may indicate that some of the Mg^{2+} in the dolomitization process came from pore water in the middle-shallow burial period.

At the same time, the Indo-Yanshanian rift tension and fracture slip facilitated the upwelling of magmatic water and the flow of stratigraphic brine, and also the superimposed modification of burial and hydrothermal action in the fractured sections, resulting in the formation of dolomite with special chemical indicators (Jiu et al., 2020). Relative hydrothermal action also affected ssD. Notably, the LHST MCD has also been affected by atmospheric freshwater compared to the EHST saddle dolomites because of karstification and the influence of fault communication with the surface (Figure 10C).

5.2 Influence of dolomitization on reservoir porosity

The physical data show that the porosities of the dolomite mainly range between 0.5% and 3%, while the permeability data are concentrated between 0.05 mD and 0.2 mD. Some of the SD and MCD samples are affected by fracture zones, such as specimens numbered DL-28-2, DL-12-1′, DS-35′and DS-37′, which can have porosity values close to or even greater than 10% (Figure 12; Supplementary Appendix S5).

In the pore-permeability covariogram (excluding the above mentioned samples with overtop values), ssD is the best dolomite in terms of physical properties and a good positive correlation, which may indicate good homogeneity of the reservoir and its matrix pore distribution (Jiang et al., 2015; Jiang et al., 2016). The samples located in the LHST have significantly better physical properties than the EHST, and the former has a greater slope. This result may indicate that the LHST ssD has better pore connectivity, and therefore makes a better contribution to the increase in permeability (Figure 12).

The other types show poor physical properties, only slightly better than those of the limestone, and are not correlated, pointing to the fact that the associated dolomitization did not result in significant physical improvement.

5.2.1 The (pene) contemporaneous stage

Microbial dolomitization in the (pene) contemporaneous stage occurred largely in the EHST period, and massive microbialites were deposited with a negative δ^{13}C shift. Microbial rocks have been shown to form potential reservoirs. However, according to the observation results (Figures 4D–F), the Changping Formation mD does not produce (pene) contemporaneous dissolutive pores, despite frequent sea-level fluctuations. The lack of a long-term unconformity in the EHST also prevents mD from forming coherent pores, and therefore, the EHST microbialites are not considered high-quality reservoirs.

DM is influenced by microbial metabolism, but mainly exhibits low-salinity sabkha dolomitization characterized by low porosity and permeability (Jiang et al., 2016), as indicated by the investigated physical data (Supplementary Appendix S5). Reflux dolomitization, however, could cause a more complex reservoir formation mechanism. Examples include the Sichuan Basin in China (Cai et al., 2014; Liu et al., 2020) and the Permian Basin in the United States (Saller, 2004). Near the restricted environment, the brine that converted directly from the sabkha and reflux effect contains sufficient or even excessive Mg^{2+}, leading to excessive dolomitization and a theoretical 75%

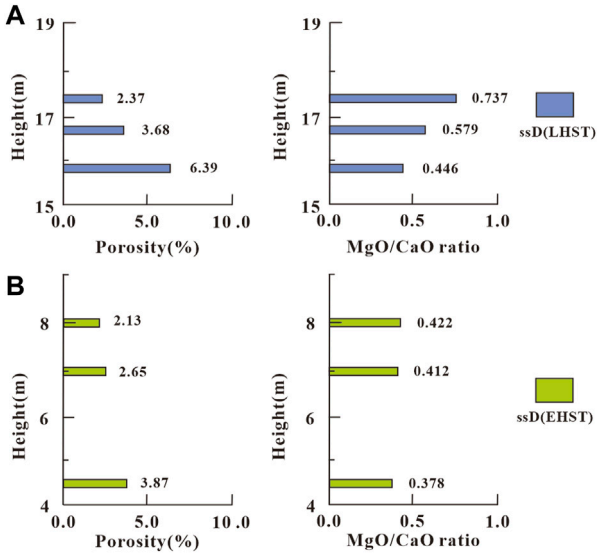

FIGURE 13
Mechanism of porosity increase in the upper changping formation, dingjiatan section. The samples in panel **(A)** are from the dingjiatan section, and those in panel **(B)** are from the miaofengshan section.

increase in dolomite volume, accompanied by a significant decrease in porosity with a main reaction of $2CaCO_3 + Mg^{2+} + CO_3^{2-} \rightarrow CaMg(CO_3)_2$ (Weyl, 1960; Pray and Murray, 1965). The dolomitization fluids far from the limited environment have lower alkalinity, and the slightly deeper stratigraphic zone also tends to reduce Mg^{2+} as the permeation proceeds. The replacement reaction is dominated by equimolar replacement, resulting in a theoretical 13% decrease in dolomite volume and the formation of intergranular pores, with a reaction equation of $2CaCO_3 + Mg^{2+} \rightarrow CaMg(CO_3)_2 + Ca^{2+}$ (Halley and Schomoker, 1983; Lucia and Major, 1994). For example, ssD samples with (pene) contemporaneous features from the LHST of the Changping Formation at 17.3 m, 16.7 m and 15.8 m (No. DH-8-1, DL-26-1, and DS-22, respectively) are all located in the Dingjiatan section, and their position in the outcrop deepens in turn and gradually moves away from the confining zone. Correspondingly, the MgO/CaO ratio decreases from 0.737 above the theoretical dolomite to 0.579 and 0.446, while the porosity increases from 2.37% to 3.68%, and ultimately 6.38% (Figure 13A).

5.2.2 The shallow-middle burial stage

During the sedimentary period of LHST, the large amount of DM indicates the influence of the (pene) contemporaneous sabkha dolomitization, followed by ssD with primary pores and reservoir skeletons, indicating reflux dolomitization. Although the ssD of the LHST is characterized by the shallow-medium burial phase mentioned above, during which dolomite grew in the annular form, the pore distribution pattern still retains the (pene) contemporaneous characteristics (Figure 13A), and the intercrystalline pores are filled with phase I oil and gas (Figure 5). These hydrocarbons are adsorbed onto the crystal surface, preventing further dolomitization and facilitating pore preservation (Jiang et al., 2015; Jiang et al., 2016). In contrast, the EHST reservoirs rely solely on middle-shallow burial dolomitization. The associated pore reduction mechanism and the accompanying changes in MgO/CaO ratios are very weak in the Miaofengshan section with sample numbers of DH-21-1, DL-32-1, and DH-9-2, respectively (Figure 13B). Despite the tendency for further concentration, as well as brine infiltration, the amount of Mg^{2+} and associated fluid flow capacity in the burial environment are limited, thus resulting in incomplete dolomitization. Their slightly better physical properties compared to those of limestone (Figure 12; Supplementary Appendix S5), however, may indicate that a few equimolar replacement mechanisms still occurred during the shallow-medium burial period, with the formation of intergranular pores filling the phase II hydrocarbon.

5.2.3 The middle-deep burial stage

During the middle-deep burial period and Yanshanian period, the strong tectonic movement produced fractures, constituted new reservoir spaces, and also provided migration channels. When the hydrocarbon and hydrothermal fluids flowed along the faults, dissolved pores were produced, and these dissolved dolomite liquids also reached the dolomite saturation state under the influence of residual high-salinity formation water. For example, in the EHST, SD partly features a poikilitic texture (Figure 4O), so the phase II oil and gas accumulated only in the residual intergranular pores and fractures. These high-temperature hydrocarbons and hydrothermal fluids also affected the early products, such as ssD in the EHST with hydrothermal geochemical indicators and petrological characteristics shown in Figure 4H, where irregularly mosaic crystals are visible in the upper left ssD.

In the LHST, apart from deep fluids, the fault that communicated with the top of the formation introduced atmospheric water into the reservoirs. Thus, the MCD underwent more abundant dolomitized fluids during the growth period compared to the SD in the EHST, and these MCD samples contain breccias with a lack of pores (Figure 4L). Although the MCD can be distributed beyond the faults, which is destructive to the nearby ssD reservoirs, the overall ssD reservoir preservation condition in EHST is still quite good as mentioned above.

In conclusion, the discovery of porous Cambrian reservoirs formed by multiphase dolomitization in this study strengthens the hypothesis that paleo-reservoirs may host significant petroleum resources for exploration. The pore-enhancement mechanism of the LHST in the early stage was conducive to the formation of high-quality reservoirs. Although some pores in ssD were removed during the shallow-middle burial period, the effective pore-retention capacity is still beneficial to the early hydrocarbon accumulation. By comparison, the less effective ssD reservoirs in the EHST were only formed in the shallow-middle burial stage with a lack of early optimal transformation. Even in the middle-deep burial stage, the late hydrocarbon could also be accumulated in the intergranular pores of SD in the EHST, the primary exploration target for the study area is still the ssD reservoir in the LHST followed by the ssD reservoir in the EHST, as the better porosity increase mechanism and considerable preservation condition of the former.

6 Conclusion

This study conducted a detailed analysis of the Cambrian Changping Formation dolomite reservoir in the Dingjiatan area of

the North China Platform. Five dolomite and dolomitization events can be identified based on lithological and geochemical characteristics. Compared with mD, which is interpreted as a typical product of (pene) contemporaneous microbial dolomitization, the absence of depleted carbon isotopic values of DM is probably caused by both microbial metabolism and an increasing sabkha interaction in the (pene) contemporaneous stage.

The elevated $^{87}Sr/^{88}Sr$ ratios and low oxygen isotopic values of the EHST ssD demonstrate shallow-middle burial dolomitization fluids related to brines of marine origin. In contrast, the LHST ssD was derived from the superimposition of (pene) contemporaneous dolomitization on a burial event, with the participation of atmospheric freshwater exhibiting a set of much lower inclusion temperature and salinity values.

MCD and SD are characterized by seawater and hydrothermal geochemistry, with shallow-middle burial pore water dolomitization superimposed on middle-deep burial hydrothermal transformation, and the former is also influenced by terrigenous water characterized by negative Eu anomalies.

The (pene) contemporaneous sabkha and reflux dolomitization were the dominant periods of reservoir formation accompanied by the porosity increase caused by reflux fluids.

The main exploration target for the study area is the ssD reservoir in the LHST, followed by the ssD reservoir in the EHST, by considering the better porosity increase mechanisms and preservation conditions of the former.

This study confirms that carbonates affected by multiphase dolomitization should be considered as prospects for petroleum exploration.

Data availability statement

The original contributions presented in the study are included in the article/Supplementary Material, further inquiries can be directed to the corresponding author.

Author contributions

YB: conceptualization and original draft; ZuZ: supervision and project administration; ZeZ: datacuration and visualization; JG: investigation.

Funding

This work is funded by Scientific Research and Technology Development Project of PetroChina Company Limited (Grant No. 2022KT0302). The funder was not involved in the study design, collection, analysis, interpretation of data, the writing of this article or the decision to submit it for publication.

Conflict of interest

Authors YB, ZuZ, ZeZ and JG were employed by the Research Institute of Petroleum Exploration & Development, PetroChina.

Publisher's note

Supplementary material

The Supplementary Material for this article can be found online at: https://www.frontiersin.org/articles/10.3389/feart.2023.1091424/full#supplementary-material

References

Adams, J. E., and Rhodes, M. L. (1960). Dolomitization by seepage refluxion. *Bull. Am. Assoc. Petroleum Geol.* 44 (12), 1912–1920.

Ahmad, W., Ullah, S., Ahmad, I., Gingras, M. K., Shafique, M., Khan, E. U., et al. (2021). Reflux dolomitization and subsequent hydrothermal dolomitization induced by the alkaline igneous province in the middle devonian nowshera formation (peshawar basin, NW Pakistan). *Mar. Petroleum Geol.* 131, 105178–105217. doi:10.1016/j.marpetgeo.2021.105178

Al-Aasm, I. S. (2000). Chemical and isotopic constraints for recrystallization of sedimentary dolomites from the Western Canada Sedimentary Basin. *Aquat. Geochem.* 6 (2), 227–248. doi:10.1023/a:1009611224589

Al-Aasm, I. S., and Crowe, R. (2018). Fluid compartmentalization and dolomitization in the cambrian and ordovician successions of the huron domain, Michigan basin. *Mar. Petroleum Geol.* 92, 160–178. doi:10.1016/j.marpetgeo.2018.02.011

Alibo, D. S., and Nozaki, Y. (1999). Rare Earth elements in seawater: Particle association, shale-normalization, and Ce oxidation. *Geochimica Cosmochimica Acta* 63 (3-4), 363–372. doi:10.1016/s0016-7037(98)00279-8

Azmy, K., Brand, U., Sylvester, P., Gleeson, S., Logan, A., and Bitner, M. A. (2011). Biogenic and abiogenic low-Mg calcite (bLMC and aLMC): Evaluation of seawater-REE composition, water masses and carbonate diagenesis. *Chem. Geol.* 280, 180–190. doi:10.1016/j.chemgeo.2010.11.007

Azmy, K., Lavoie, D., Knight, I., and Chi, G. (2008). Dolomitization of the Lower Ordovician Aguathuna Formation carbonates, Port au Port Peninsula, Western Newfoundland, Canada: implications for a hydrocarbon reservoir. *Can. J. Earth Sci.* 45 (7), 795–813. doi:10.1139/e08-020

Azmy, K., Veizer, J., Misi, A., de Oliveira, T. F., Sanches, A. L., and Dardenne, M. A. (2001). Dolomitization and isotope stratigraphy of the vazante formation, sao francisco basin, Brazil. *Precambrian Res.* 112 (3-4), 303–329. doi:10.1016/s0301-9268(01)00194-2

Bai, Y., Li, J. Z., Liu, W., Xu, Z. H., Xu, W. L., Li, X., et al. (2021a). Characteristics and multiple dolomitization mode of the Lower Cambrian dolomite reservoir, northwestern Tarim Basin. *Acta Pet. Sin.* 42 (9), 1174–1191.

Bai, Y., Luo, P., Liu, W., Xu, A. N., Zhao, Z. Y., Wang, S., et al. (2019). Characteristics and origin of oncolite from Changping Formation in the series 2 of cambrian in western beijing. *Geoscience* 33 (3), 587–597.

Bai, Y., Luo, P., Xu, W. L., Wang, S., and Gong, J. Y. (2021b). Characteristics and genesis of thrombolites in the cambrian Changping Formation,series 2,Beijing. *Acta Sedimentol. Sin.* 39 (4), 873–885.

Baniak, G. M., Amskold, L., Konhauser, K. O., Muehlenbachs, K., Pemberton, S. G., and Gingras, M. K. (2014). Sabkha and burrow-mediated dolomitization in the mississippian debolt formation, northwestern alberta, Canada. *Ichnos* 21, 158–174. doi:10.1080/10420940.2014.930036

Banner, J. L., Hanson, G. N., and Meyers, W. J. (1998). Rare Earth element and Nd isotopic variations in regionally extensive dolomites from the burlington-keokuk formation (mississippian): Implications for REE mobility during carbonate diagenesis. *J. Sediment. Petrology* 58, 4150–4433.

Bau, M., and Dulski, P. (1965). Distribution of yttrium and rare-Earth elements in the penge and kuruman iron-formations, transvaal supergroup, south Africa. *Precambrian Res.* 79 (1-2), 37–55. doi:10.1016/0301-9268(95)00087-9

Bau, M. (1991). Rare-Earth element mobility during hydrothermal and metamorphic fluid-rock interaction and the significance of the oxidation state of europium. *Chem. Geol.* 93 (3-4), 219–230. doi:10.1016/0009-2541(91)90115-8

Bodnar, R. J. (2003). "Reequilibration of fluid inclusions," in *Fluid inclusions—analysis and interpretation; special publication*. Editors I. Sampson, A. Anderson, and D. Marshall (Ottawa: Mineralogical Association of Canada), Vol. 32, 213–231.

Brand, U., and Veizer, J. (1980). Chemical diagenesis of a multicomponent carbonate system; 1, Trace elements. *J. Sediment. Petrology* 50 (4), 1219–1236.

Budd, D. A. (1997). Cenozoic dolomites of carbonate islands: Their attributes and origin. *Earth-Science Rev.* 42 (1-2), 1–47. doi:10.1016/s0012-8252(96)00051-7

Burke, W., Denison, R., Hetherington, E., Koepnick, R., Nelson, H., and Otto, J. (1982). Variation of seawater $^{87}Sr/^{86}Sr$ throughout Phanerozoic time. *Geology* 10, 516–519. doi:10.1130/0091-7613(1982)10<516:vosstp>2.0.co;2

Cai, C. F., He, W. X., Jiang, L., Li, K., Xiang, L., and Jia, L. (2014). Petrological and geochemical constraints on porosity difference between Lower Triassic sour- and sweet-gas carbonate reservoirs in the Sichuan Basin. *Mar. Petroleum Geol.* 56, 34–50. doi:10.1016/j.marpetgeo.2014.04.003

Carpenter, S. J., Lohmann, K. C., Holden, P., Walter, L. M., Huston, T. J., and Halliday, A. N. (1991). $\delta^{18}O$ values, $^{87}Sr/^{86}Sr$ and Sr/Mg ratios of late devonian abiotic marine calcite: Implications for the composition of ancient seawater. *Geochimica cosmochimica acta* 55 (7), 1991–2010. doi:10.1016/0016-7037(91)90038-7

Cui, Y. Q., Wang, J. G., Tian, J. Z., Zhao, Z. J., Xiao, Y., Wang, P. X., et al. (2018). Reservoir characteristcs and main controlling factors of Cambrian-Ordovician dolomite in the north central part of North China Platform. *Acta Pet. Sin.* 39 (8), 890–901.

Davies, G. R., and Smith, L. B. (2006). Structurally controlled hydrothermal dolomite reservoir facies: An overview. *AAPG Bull.* 90 (11), 1641–1690. doi:10.1306/05220605164

Denison, R., Koepnick, R., Burke, W., Hetherington, E., and Fletcher, A. (1997). Construction of the silurian and devonian seawater $^{87}Sr/^{86}Sr$ curve. *Chem. grology* 140, 109–121. doi:10.1016/s0009-2541(97)00014-4

Feng, Z. Z., Zhang, Y. S., and Jin, Z. K. (1998). Type, origin, and reservoir characteristics of dolostones of the ordovician Majiagou group, Ordos, north China platform. *Sediment. Geol.* 118 (1-4), 127–140. doi:10.1016/s0037-0738(98)00009-8

Friedman, G. M. (2007). Structurally controlled hydrothermal dolomite reservoir facies: An overview: Discussion. *AAPG Bull.* 91 (9), 1339–1341. doi:10.1306/04300706142

Galy, A., Yoffe, O., Janney, P. E., Williams, R. W., Cloquet, C., Alard, O., et al. (2003). Magnesium isotope heterogeneity of the isotopic standard SRM980 and new reference materials for magnesium-isotope-ratio measurements. *J. Anal. Atomic Spectrom.* 18, 1352–1356. doi:10.1039/b309273a

Goldsmith, J. R., and Graf, D. L. (1958). Structural and compositional variations in some natural dolomites. *J. Geol.* 66 (6), 678–693. doi:10.1086/626547

Goldstein, R. H., and Reynolds, T. J. (1994). Systematics of fluid inclusions in diagenetic minerials. *SEPM Short. Course* 31, 199.

Guo, Q. H., Jin, Z. K., Zhu, X. E., Chang, R., Jiang, M. Y., and Wang, J. Y. (2019). Diagenetic evolution and exploration prospect of oolitic bank in cambrian Zhangxia Formation at xiaweidian area, beijing. *Geoscience* 33 (4), 820–830.

Guo, Q. H., Jin, Z. K., Zhu, X. E., and Wang, J. Y. (2018). Characteristics of oolites and their dolomitization mechanism of the cambrian Zhangxia Formation at xiaweidian outcrop in beijing. *Geoscience* 32 (4), 766–773.

Haas, J. R., Shock, E. L., and Sassani, D. C. (1995). Rare-earth elements in hydrothermal systems - estimates of standard partial molal thermodynamic properties of aqueous complexes of the rare-earth elements at high-pressures and temperatures. *Geochimica Cosmochimica Acta* 59 (21), 4329–4350. doi:10.1016/0016-7037(95)00314-p

Halley, R. B., and Schomoker, J. W. (1983). High-porosity Cenozoic carbonate rocks of south Florida: Progressive loss of porosity with depth. *AAPG Bull.* 67 (2), 191–200.

Hao, L. R., Yang, D. B., Xu, W. L., Mu, M. S., Quan, Z. K., Yang, H. T., et al. (2020). Late Neoarchean magmatism and crustal growth in northeastern North China Craton: Constraints from zircon U-Pb-Hf isotope, trace elements and whole rock geochemistry. *Acta Petrol. Sin.* 36 (4), 1076–1090. doi:10.18654/1000-0569/2020.04.07

Hein, J. R., Gray, S. C., Richmond, B. M., and White, L. D. (1992). Dolomitization of quaternary reef limestone, aitutaki, Cook Islands. *Sedimentology* 39 (4), 645–661. doi:10.1111/j.1365-3091.1992.tb02142.x

Heydari, E. (1997). The role of burial diagenesis in hydrocarbon destruction and H2S accumulation, upper Jurassic Smackover Formation, Black Creek Field, Mississippi. *AAPG Bull.* 81, 26–45.

Hiatt, E. E., and Pufahl, P. K. (2014). "Cathodoluminescence petrography of carbonate rocks: Application to understanding diagenesis, reservoir quality, and pore system evolution," in *Cathodoluminescence and its application to geoscience; short course series*. Editor I. M. Coulson (Québec, QC, Canada: Mineralogical Association of Canada), Vol. 45, 75–96.

Hippler, D., Buhl, D., Witbaard, R., Richter, D. K., and Immenhauser, A. (2009). Towards a better understanding of magnesium-isotope ratios from marine skeletal carbonates. *Geochimica Cosmochimica Acta* 73 (20), 6134–6146. doi:10.1016/j.gca.2009.07.031

Hong, D. V., Wang, T., Tong, Y., and Wang, X. X. (2003). Mesozoic granitoids from North China Block and Qingling-Dabie-Sulu orogenic belt and their deep dynamic process. *Earth Sci. Front.* 10 (3), 231–256.

Hood, A. V. S., and Wallace, M. W. (2015). Extreme ocean anoxia during the Late Cryogenian recorded in reefal carbonates of Southern Australia. *Precambrian Res.* 261, 96–111. doi:10.1016/j.precamres.2015.02.008

Huang, Q. Y. (2014). *Dolomitization and origin of the cambrian-ordovician dolomite reservoirs in the central uplift, Tarim Basin*. Chengdu, China: Chengdu University of Technology, 1–145.

Huang, Q. Y., Liu, W., Zhang, Y. Q., Shi, S. Y., and Wang, K. (2016). Geochemistry and evolution of dolomitizing fluids of the upper cambrian-lower ordovician dolostones in central uplift, Tarim Basin. *J. Palaeogeogr.* 18 (4), 661–676.

Huang, S. J., Qing, H. R., Pei, C. R., Hu, Z. W., Wu, S. J., and Sun, Z. L. (2006). Strontium concentration,isotope composition and dolomitization fluids in the feixianguan formation of Triassic,Eastern sichuan of China. *Acta Petrol. Sin.* 22 (8), 2123–2132.

Jiang, L., Cai, C. F., Wordern, R. H., Crowley, S. F., Jia, L., Zhang, K., et al. (2016). Multiphase dolomitization of deeply buried Cambrian petroleum reservoirs, Tarim Basin, north-west China. *Sedimentology* 63 (7), 2130–2157. doi:10.1111/sed.12300

Jiang, L., Pan, W. Q., Cai, C. F., Jia, L. Q., Pan, L. Y., Wang, T. K., et al. (2015). Fluid mixing induced by hydrothermal activity in the Ordovician carbonates in Tarim Basin, China. *Geofluids.* 15 (3), 483–498. doi:10.1111/gfl.12125

Jiang, L., Worden, R. H., Cai, C. F., Li, K., Xiang, L., Cai, L., et al. (2014). Dolomitization of gas reservoirs: The upper permian changxing and lower triassic feixianguan formations, northeast Sichuan Basin, China. *J. Sediment. Res.* 84 (10), 792–815. doi:10.2110/jsr.2014.65

Jiang, L., Xu, Z. H., Shi, S. Y., and Liu, W. (2019). Multiphase dolomitization of a microbialite-dominated gas reservoir, the middle triassic leikoupo formation, Sichuan Basin, China. *J. Petroleum Sci. Eng.* 180, 820–834. doi:10.1016/j.petrol.2019.05.014

Jiu, B., Huang, W. H., Mu, N. N., and He, M. Q. (2020). Effect of hydrothermal fluids on the ultra-deep Ordovician carbonate rocks in Tarim Basin, China. *J. Petroleum Sci. Eng.* 194, 107445–107518. doi:10.1016/j.petrol.2020.107445

Jones, G. D., and Xiao, Y. (2005). Dolomitization, anhydrite cementation, and porosity evolution in a reflux system: Insights from reactive transport models. *AAPG Bull.* 89, 577–601. doi:10.1306/12010404078

Kaczmarek, S. E., and Sibley, D. F. (2011). On the evolution of dolomite stoichiometry and cation order during high-temperature synthesis experiments: An alternative model for the geochemical evolution of natural dolomites. *Sediment. Geol.* 240, 30–40. doi:10.1016/j.sedgeo.2011.07.003

Kareem, K. H., Al-Aasm, I. S., and Mansurbeg, H. (2021). Geochemical constraints of hydrothermal alteration of dolostones: An example of lower cretaceous qamchuqa formation, kurdistan region, northern Iraq. *Mar. Petroleum Geol.* 134, 105337. doi:10.1016/j.marpetgeo.2021.105337

Kawabe, I., Toriumi, T., Ohta, A., and Miura, N. (1998). Monoisotopic REE abundances in seawater and the origin of seawater tetrad effect. *Geochem. J.* 32 (4), 213–229. doi:10.2343/geochemj.32.213

Keith, M. L., and Weber, J. N. (1964). Carbon and oxygen isotopic composition of selected limestones and fossils. *Geochimica Cosmochimica Acta* 28 (10-11), 1787–1816. doi:10.1016/0016-7037(64)90022-5

Kırmacıa, M. Z., Yıldıza, M., Kandemirb, R., and Eroğlu-Gümrüka, T. (2018). Multistage dolomitization in late jurassic–early cretaceous platform carbonates (berdiga formation), başoba yayla (trabzon), NE Turkey: Implications of the generation of magmatic arc on dolomitization. *Mar. Petroleum Geol.* 89, 515–529. doi:10.1016/j.marpetgeo.2017.10.018

Kucera, J., Cempirek, J., Dolnicek, Z., Muchez, P., and Prochaska, W. (2009). Rare Earth elements and yttrium geochemistry of dolomite from post-Variscan vein-type mineralization of the Nízký Jeseník and Upper Silesian Basins, Czech Republic. *Czech Repub. J. Geochem. Explor.* 103, 69–79. doi:10.1016/j.gexplo.2009.08.001

Liu, D., Cai, C., Hu, Y., Jiang, L., Peng, Y., Yu, R., et al. (2020). Multi-stage dolomitization process of deep burial dolostones and its influence on pore evolution: A case study of longwangmiao Formation in the lower cambrian of central Sichuan Basin. *J. China Univ. Min. Technol.* 49 (6), 1150–1165.

Liu, H., Shi, P. Z., Tang, H. M., Wang, Z. Y., Shang, T., Zhao, Z. J., et al. (2021). Dolomitization of the middle ordovician Ma55 sub-member of the Majiagou Formation and implicaions for hydrocarbon exploration in the northern Ordos Basin, NW China. *Carbonates Evaporites* 36 (14), 1–14.

Lucia, F. J., and Major, R. P. (1994). Porosity evolution through hypersaline reflux dolomitization. *Dolomites Int. Assoc. Sedimentologists Special Publ.* 21, 325–341. doi:10.1002/9781444304077.ch18

Lukoczki, G., Haas, J., Gregg, J. M., Machel, H. G., Kele, S., and John, C. M. (2019). Multi-phase dolomitization and recrystallization of Middle Triassic shallow marine-peritidal carbonates from the Mecsek Mts. (SW Hungary), as inferred from petrography, carbon, oxygen, strontium and clumped isotope data. *Mar. Petroleum Geol.* 101, 440–458. doi:10.1016/j.marpetgeo.2018.12.004

Machel, H. G. (2014). "Concepts and models of dolomitization: A critical reappraisal," in *The geometry and petrigenesis of dolomite hydrocarbon reservoirs*. *Geological society london special publications*. Editor C. J. R. Braithwaite, Vol. 235, 7–63.1

Mahboubi, A., Nowrouzi, Z., Al-Aasm, I. S., Moussavi-Harami, R., and Mahmudy-Gharaei, M. H. (2016). Dolomitization of the silurian niur formation, tabas block, east central Iran: Fluid flow and dolomite evolution. *Mar. Petroleum Geol.* 77, 791–805. doi:10.1016/j.marpetgeo.2016.07.023

Malone, M. J., and Paul, A. (1996). Hydrothermal dolomitization and recrystallization of dolomite breccias from the Miocene Monterey Formation, Tepusquet area, California. *J. Sediment. Petrology* 66 (5), 976–990.

Mansurbeg, H., Alsuwaidi, M., Salih, N., Shahrokhi, S., and Morad, S. (2021). Integration of stable isotopes, radiometric dating and microthermometry of saddle dolomite and host dolostones (cretaceous carbonates, kurdistan, Iraq): New insights into hydrothermal dolomitization. *Mar. Petroleum Geol.* 127, 104989. doi:10.1016/j.marpetgeo.2021.104989

Mavromatis, V., Gautier, Q., Bosc, O., and Schott, J. (2013). Kinetics of Mg partition and Mg stable isotope fractionation during its incorporation in calcite. *Geochimica Cosmochimica Acta* 114, 188–203. doi:10.1016/j.gca.2013.03.024

Mavromatis, V., Meister, P., and Oelkers, E. H. (2014). Using stable Mg isotopes to distinguish dolomite formation mechanisms: A case study from the Peru margin. *Chem. Geol.* 385, 84–91. doi:10.1016/j.chemgeo.2014.07.019

Mei, M. X. (2011). Depositional trends and sequence-stratigraphic successions under the cambrian second-order transgressive setting in the North China platform: A case study of the xiaweidian section in the Western suburb of beijing. *Geol. China* 38 (2), 317–337.

Meng, X. H., and Ming, G. E. (2003). Cyclic sequences, events and evolution of the sino-Korean plate, with a discussion on the evolution of molar-tooth carbonates, phosphorites and source rocks. *Acta Geol. Sin.* 77 (3), 382–401. doi:10.1111/j.1755-6724.2003.tb00754.x

Morad, S., Al-Ramadan, K., De, Ros. F., and Ketzer, J. M. (2010). The impact of diagenesis on spatial and temporal distribution of reservoir heterogeneity in sandstones, links to depositional facies and sequence stratigraphy. *Am. Assoc. Petroleum Geol. Special Publ.* 94, 1267–1309.

Morad, S. (1998). "Carbonate cementation in sandstones, distribution patterns and geochemical evolution," in *Carbonate cementation in sandstones. International association of sedimentologists (IAS) special publication*. Editor S. Morad, Vol. 26, 1–26.

Muhammad, R., Tehseen, Z., Khalid, L., Shahid, G., and Enzhao, X. (2020). Petrographic and rare Earth elemental characteristics of Cambrian Girvanella oncoids exposed in the North China Platform: Constraints on forming mechanism, REE sources, and paleoenvironments. *Arabian J. Geosciences* 13 (858), 1–15.

Pogge von Strandmann, P. A. E., Burton, K. W., James, R. H., van Calsteren, P., Gislason, S. R., and Sigfússon, B. (2008). The influence of weathering processes on riverine magnesium isotopes in a basaltic terrain. *Earth Planet. Sci. Lett.* 276 (1-2), 187–197. doi:10.1016/j.epsl.2008.09.020

Pogge von Strandmann, P. A. E. (2008). Precise magnesium isotope measurements in core top planktic and benthic foraminifera. *Geochem. Geophys. Geosystems* 9 (12), Q12015. doi:10.1029/2008gc002209

Pray, L. C., and Murray, R. C. (1965). Dolomitization and limestone diagenesis. *Gulhane Med. J.* 48 (3), 137–141.

Qian, Y. X., Wu, H. Z., Zhou, L. F., Huang, K. J., Deng, M. Z., Li, Y., et al. (2019). Characteristic and origin of dolomites in the third and fourth members of Leikoupo Formation of the Middle Triassic in NW Sichuan Basin: Constraints in mineralogical, petrographic and geochemical data. *Acta Petrol. Sin.* 35 (4), 1161–1180.

Qiao, Z. F., Shao, G. M., Luo, X. Y., Cao, P., Sun, X. W., and Shen, A. J. (2021). Genetic classification and large-scale reservoir development law of burial dolomite: Cognition based on LA-ICP-MS trace elemental mapping and U-Pb dating. *Nat. Gas. Ind.* 41 (9), 46–56.

Saller, A. H. (2004). Palaeozoic dolomite reservoirs in the Permian Basin, SW USA: Stratigraphic distribution, porosity, permeability and production. *Geol. Soc. Lond. Spec. Publ.* 235 (1), 309–323. doi:10.1144/gsl.sp.2004.235.01.13

Sauer, P. E., Miller, G. H., and Overpeck, J. T. (2001). Oxygen isotope ratios of organic matter in arctic lakes as a paleoclimate proxy: Field and laboratory investigations. *J. Paleolimnol.* 25 (1), 43–64. doi:10.1023/a:1008133523139

Schott, J., Mavromatis, V., Fujii, T., Pearce, C. R., and Oelkers, E. H. (2016). The control of carbonate mineral Mg isotope composition by aqueous speciation: Theoretical and experimental modeling. *Chem. Geol.* 445, 120–134. doi:10.1016/j.chemgeo.2016.03.011

Shields, G., and Stille, P. (2001). Diagenetic constraints on the use of cerium anomalies as palaeoseawater redox proxies: An isotopic and REE study of cambrian phosphorites. *Chem. Geol.* 175, 29–48. doi:10.1016/s0009-2541(00)00362-4

Sumrall, J., Mylroie, J., and Kambesis, P. (2015). Microbial mixing zone dolomitization and karst development within Isla de Mona Dolomite, Isla de Mona, Puerto Rico. *Carbonates Evaporites* 30 (1), 45–58. doi:10.1007/s13146-014-0198-1

Swart, P. K., Cantrell, D. L., Westphal, H., Handford, C. R., and Kendall, C. G. (2005). Origin of dolomite in the Arab-D reservoir from the Ghawar field, Saudi Arabia: Evidence from petrographic and geochemical constraints. *J. Sediment. Res.* 75 (3), 476–491. doi:10.2110/jsr.2005.037

Swart, P. K. (2015). The geochemistry of carbonate diagenesis: The past, present and future. *Sedimentology* 62, 1233–1304. doi:10.1111/sed.12205

Tipper, E. T., Galy, A., and Bickle, M. J. (2006b). Riverine evidence for a fractionated reservoir of Ca and Mg on the continents: Implications for the oceanic Ca cycle. *Earth Planet. Sci. Lett.* 247 (3-4), 267–279. doi:10.1016/j.epsl.2006.04.033

Tipper, E. T., Galy, A., Gaillardet, J., Bickle, M. J., Elderfield, H., and Carder, E. A. (2006a). The magnesium isotope budget of the modern ocean: Constraints from riverine magnesium isotope ratios. *Earth Planet. Sci. Lett.* 250 (1-2), 241–253. doi:10.1016/j.epsl.2006.07.037

Tortola, M., Al-Aasm, I. S., and Crowe, R. (2020). Diagenetic pore fluid evolution and dolomitization of the silurian and devonian carbonates, huron domain of southwestern ontario: Petrographic, geochemical and fluid inclusion evidence. *Minerals* 10 (2), 140. doi:10.3390/min10020140

Vahrenkamp, V. C., and Swart, P. K. (1990). New distribution coefficient for the incorporation of strontium into dolomite and its implications for the formation of ancient dolomites. *Geology* 18, 387–391. doi:10.1130/0091-7613(1990)018<0387:ndcfti>2.3.co;2

Vasconcelos, C., Bernasconi, S., Grujic, D., Tien, A. J., and Mckenzie, J. A. (1995). Microbial mediation as a possible mechanism for natural dolomite formation at low temperatures. *Nature* 377, 220–222. doi:10.1038/377220a0

Vasconcelos, C., and McKenzie, J. A. (1997). Microbial mediation of modern dolomite precipitation and diagenesis under anoxic conditions (Lagoa Vermelha, Rio de Janeiro, Brazil). *J. Sediment. Res.* 67 (3), 378–390.

Weyl, P. K. (1960). Porosity through dolomitization: Conservation of mass requirements. *J. Sediment. Petrology* 30 (1), 85–90.

Whitaker, F. F., and Xiao, Y. (2010). Reactive transport modeling of early burial dolomitization of carbonate platforms by geothermal convection. *AAPG Bull.* 94, 889–917. doi:10.1306/12090909075

William, J. M. (1989). Trace element and isotope geochemistry of zoned calcite cements, lake valley formation (mississippian, new Mexico): Insights from water-rock interaction modelling. *Sediment. Geol.* 65 (3-4), 355–370. doi:10.1016/0037-0738(89)90034-1

Xiao, F. (2020). *Sequence stratigraphy and lithofacies paleogeography of the Cambrian in the middle-eastern North China Platform*. Wuhan, China: China University of Geoeciences, 1–172.

Xu, W. L., Li, J. Z., Liu, X. S., Li, N, X., Zhang, C. L., Zhang, Y. Q., et al. (2021). Accumulation conditions and exploration directions of Ordovician lower assemblage natural gas, Ordos Basin, NW China. *Petroleum Explor. Dev.* 48 (3), 641–654. doi:10.1016/s1876-3804(21)60051-4

Yan, W. (2019). *Karst types and karst models of the lower paleozoic in the Jizhong depression, north China*. Beijing: China University of Petroleum, 1–112.

You, X. L., Sun, S., Zhu, J. Q., Liu, L., and He, K. (2011). Progress in the study of microbial dolomite model. *Earth Sci. Front.* 18 (4), 52–64.

Yu, Y., Chen, Y. L., Li, D. P., and Su, J. T. (2022). A transient oxygen increase in the mesoproterozoic ocean at ~1.44 Ga: Geochemical evidence from the tieling formation, north China platform. *Precambrian Res.* 369, 1–12.

Zhao, H., and Jones, B. (2012b). Genesis of fabric-destructive dolostones: A case study of the brac formation (oligocene), cayman brac, British west indies. *Sediment. Geol.* 267-268, 36–54. doi:10.1016/j.sedgeo.2012.05.007

Zhao, H., and Jones, B. (2012a). Origin of "island dolostones": A case study from the cayman formation (miocene), cayman brac, brBritishest indies. *Sediment. Geol.* 243-244, 191–206. doi:10.1016/j.sedgeo.2011.11.004

Zhao, X. Z., Jin, F. M., Wang, Q., and Bai, G, P. (2015). Buried-hill play, Jizhong subbasin, bohai bay basin: A review and future propespectivity. *AAPG Bull.* 99 (1), 1–26. doi:10.1306/07171413176

Zhemchugova, V. A., Evdokimov, N. V., Poort, J., and Akhmanov, G. G. (2020). Lower Permian carbonate buildups in the northern Timan-Pechora Basin as the main hydrocarbon exploration object. *Lithology Mineral Resour.* 55 (4), 245–260. doi:10.1134/s0024490220040069

Nomenclature

CL, Cathodoluminescence; DM, Dolomicrite; DSM3, Dead Sea Magnesium Ltd., Israel; EHST, Early highstand systems tract; FIAs, Fluid-inclusions assemblages; FO1, Frequency of Oil Inclusions; HREE, Heavy rare earth element; LHST, Late highstand systems tract; LREE, Light rare earth element; MCD, Medium to coarse crystalline dolomite; mD, Microbial dolomite; REE, Rare earth element; SD, Saddle dolomite; SEM, Scanning electron microscope; ssD, Structureless dolomite; T_h, Homogenization temperature; TST, Transgressive systems tract; VPDB, Vienna Pee Dee Belemnite; XRD, X-ray diffraction.